

NASA TECHNICAL NOTE



NASA TN D-3028

e. 1

NASA TN D-3028



TECH LIBRARY KAFB, NM

MAIL ROOM
AUG 11 1965
KAFB, NM

ANALYTICAL INVESTIGATION OF A HELICOPTER ROTOR DRIVEN AND CONTROLLED BY A JET FLAP

by William T. Evans and John L. McCloud III

Ames Research Center

Moffett Field, Calif.





ANALYTICAL INVESTIGATION OF A HELICOPTER ROTOR DRIVEN
AND CONTROLLED BY A JET FLAP

By William T. Evans and John L. McCloud III

Ames Research Center
Moffett Field, Calif.

NATIONAL AERONAUTICS AND SPACE ADMINISTRATION

For sale by the Clearinghouse for Federal Scientific and Technical Information
Springfield, Virginia 22151 - Price \$2.00

ANALYTICAL INVESTIGATION OF A HELICOPTER ROTOR DRIVEN
AND CONTROLLED BY A JET FLAP

By William T. Evans and John L. McCloud III
Ames Research Center

SUMMARY

Results of a theoretical study of the characteristics of a particular jet-flat rotor are presented and analyzed. The study made extensive use of high-speed digital computations. It was found that the momentum and power coefficients varied significantly with shaft angle for many flight conditions. This finding is rationalized, and its significance explored. It was also found that higher harmonic control of the flap reduced higher harmonics of blade flapping, thrust, and torque.

The study indicated that higher speeds can be attained in pure helicopter flight than with any conventional rotor. It further indicated that the maximum attainable speed in such flight is likely to be higher if theoretical supercirculatory thrust recovery on the blade is not realized in practice.

INTRODUCTION

The concept of driving and controlling a helicopter rotor by a variably deflectable jet flap has been proposed (refs. 1 and 2). Such a design offers at least three potential advantages: (1) mechanical simplification due to the substitution of jet-flap control for conventional blade-pitch control, (2) increased lift and propulsive force due to jet-induced "supercirculation," and (3) reduced vibrations due to higher harmonic control of the jet flap. Applications to three types of pure helicopter have been suggested: (1) a high-speed, low-drag vehicle ($V > 200$ knots), (2) an efficient medium-speed vehicle, and (3) a crane helicopter.

The present investigation was undertaken to study the theoretical characteristics of a jet-flap rotor. Because of the complexity of the problem, the study was based primarily on the results of high-speed digital computations. Three versions of a computer program were written and are described herein. The programs are general, the first two being applicable to jet-driven or jet-augmented rotors of almost any design, and the third being applicable to shaft-driven rotors only. The third program was used to permit comparisons of jet-flap and conventional rotors.

It should be emphasized that this concept of the jet-flap rotor includes the notion of complete control by jet deflection alone, that is, the blade pitch is fixed. In a manner entirely analogous to conventional collective and cyclic pitch control, "collective" and "cyclic" jet deflections can be defined and given analogous notation. Thus, in this report, the jet-deflection angle δ is given as

$$\delta = \bar{A}_0 - \bar{A}_1 \cos \psi - \bar{B}_1 \sin \psi - \bar{A}_2 \cos 2\psi - \dots \quad (1)$$

where \bar{A}_0 is termed the "collective" jet deflection, \bar{A}_1 the "lateral cyclic" jet deflection, \bar{B}_1 the "longitudinal cyclic" jet deflection, and the higher order coefficients "higher harmonic control" parameters.

Of importance in the study is an over-all jet momentum coefficient C_{jR} . Although it is a force coefficient, it can be expected to correlate well with the rotor power coefficient, C_P , since the rotor is entirely jet propelled. The jet-momentum coefficient is therefore emphasized in this report. Problems of internal flow, however, are not examined.

NOTATION

\bar{A}_0	average or "collective" jet deflection, deg
\bar{A}_i, \bar{B}_i	harmonic coefficients of jet deflection, deg, $\delta = \bar{A}_0 - \bar{A}_1 \cos \psi - \bar{B}_1 \sin \psi - \bar{A}_2 \cos 2\psi - \dots$
A_N	nozzle area of jet flap (all blades), ft ²
A_1, B_1	lateral and longitudinal cyclic pitch, respectively, deg
a_i, b_i	harmonic coefficients of blade flapping, deg, $\beta = a_0 - a_1 \cos \psi - b_1 \sin \psi - a_2 \cos 2\psi - \dots$
B	tip loss factor, 0.99 for jet-flap rotor, 0.98 for shaft-driven rotor
b	number of blades
C_H	rotor longitudinal force coefficient, $\frac{H}{\rho(\Omega R)^2 \pi R^2}$
C_{jR}	rotor jet-momentum coefficient, $\frac{M_j V_j}{\rho(\Omega R)^2 \pi R^2}$
C_{LR}	rotor lift coefficient, $\frac{L}{\rho(\Omega R)^2 \pi R^2}$
C_{mass}	rotor mass-flow coefficient, $\frac{M_j}{\rho \Omega R \pi R^2}$
C_P	summation of component power coefficients, $C_{P_{COR}} + C_{P_i} + C_{P_o} + C_{P_P}$
$C_{P_{COR}}$	Coriolis power coefficient, computed as $C_{Q_{COR}}$

- C_{P_i} induced power coefficient, $\frac{(C_{L_R})^2}{2(V/\Omega R)}$
- C_{P_o} profile power coefficient, $\frac{2}{n} \int_{x_c}^1 \sum_{\psi} \sigma_x |u|^3 c_{d_o} dx$
- C_{P_P} propulsive power coefficient, $C_{X_R} \left(\frac{V}{\Omega R} \right)$
- C_Q shaft torque coefficient, $\frac{Q}{\rho(\Omega R)^2 \pi R^2 R}$
- $C_{Q_{COR}}$ Coriolis torque coefficient, $\frac{2(\Omega R)R \int_0^1 x m_{rad} dx}{\rho(\Omega R)^2 \pi R^2 R}$
- C_X propulsive force coefficient, $\frac{X}{q \pi R^2}$
- C_{X_R} rotor propulsive force coefficient, $\frac{X}{\rho(\Omega R)^2 \pi R^2}$
- c local blade chord, ft
- c_d total local section drag coefficient, $\frac{d}{q_l c}$
- c_{d_o} drag coefficient due to section shape (no jet effects)
- c_e equivalent blade chord (on thrust basis), $\frac{\int_{r_c}^{BR} cr^2 dr}{\int_{r_c}^{BR} r^2 dr}$, ft
- c_e' equivalent blade chord (on thrust-moment basis), $\frac{\int_{r_c}^{BR} cr^3 dr}{\int_{r_c}^{BR} r^3 dr}$, ft
- c_j local section momentum coefficient, $\frac{m_j V_j}{q_l c}$
- c_l total local section lift coefficient, $\frac{l}{q_l c}$
- c_{l_o} lift coefficient due to section shape (no jet effects)
- d total local section drag per unit span, lb/ft

e	offset of flapping hinge, ft
g	acceleration of gravity, ft/sec ²
H	downwind force perpendicular to shaft, lb
I _h	mass moment of inertia about flapping hinge, slug-ft ²
L	lift, lb
l	total local section lift per unit span, lb/ft
M	Mach number
M _j	total mass flow per second through all blades, slugs/sec
M _T	thrust moment of blade about flapping hinge, ft-lb
M _W	weight moment of blade about flapping hinge at $\beta = 0$, ft-lb
m _j	jet mass flux per unit span, all blades, slugs/ft/sec
m _{rad}	radial mass flux at a given radial station, all blades, slugs/sec
n	number of azimuth positions used in computation
Q	shaft torque, ft-lb
q	free-stream dynamic pressure, $\frac{1}{2} \rho V^2$, lb/ft ²
q _z	local dynamic pressure, $\frac{1}{2} \rho U^2$, lb/ft ²
R	rotor radius, ft
r	radial distance along blade from hub, ft
s _d	supercirculation thrust parameter, see equation (7)
s _z	supercirculation lift parameter, see equation (6)
T	thrust along shaft axis, lb
T _{DUCT}	internal temperature of blowing duct, °F
U	local velocity perpendicular to blade span, ft/sec
u	dimensionless local velocity, U/ΩR
V	free-stream velocity, ft/sec
V _j	jet velocity, ft/sec

$\frac{V}{\Omega R}$	advance ratio
v_T	induced velocity in T-direction, ft/sec
v_H	induced velocity in H-direction, ft/sec
X	propulsive force, positive upstream, lb
x	dimensionless radial station, r/R
α	local section angle of attack, deg
α_S	shaft angle, positive rearward from the vertical, deg
β	blade flapping angle with respect to shaft positive upward, deg
γ'	mass constant of blade, $\rho c_e \frac{R^4}{I_h}$
Δc_{d_j}	jet-reaction increment to section drag coefficient
Δc_{d_s}	supercirculation increment to section drag coefficient
Δc_{l_j}	jet-reaction increment to section lift coefficient
Δc_{l_s}	supercirculation increment to section lift coefficient
Δx_j	spanwise extent of slot in terms of x
δ	jet deflection, positive downward from chordline, deg
η	offset parameter, $\frac{e}{g} \frac{M_W}{I_h}$
$\theta_{0.7}$	collective pitch of blade at $x = 0.7$, deg
λ	inflow ratio, $\frac{V \sin \alpha_S - v_T}{\Omega R}$
μ	tip-speed ratio, $\frac{V \cos \alpha_S - v_H}{\Omega R}$
ρ	free-stream air density, slugs/ft ³
σ	rotor solidity, $\frac{bc_e}{\pi R}$
σ_x	local solidity, $\frac{bc}{\pi R}$

ψ azimuth station, from rear in direction of rotation, deg
 Ω rotational velocity of rotor, rads/sec

Subscripts

c cutout (at 0.111R)
max maximum
 ψ at azimuth position ψ

DESCRIPTION OF COMPUTER PROGRAMS

Flow charts for the jet-flap rotor programs are shown in figure 1.

The basic computational approach is that of reference 3, wherein a blade flapping pattern is assumed, the resulting thrust moment is calculated and harmonically analyzed, the flapping is then revised and the thrust moment recalculated, and so on, until the iteration repeats within the meaningful accuracy of the computations. Simultaneously with the flapping revisions, the momentum coefficient C_{jR} is also revised until the shaft torque is essentially zero (the required equilibrium condition). (This simultaneous iteration on flapping pattern and C_{jR} has proven quite feasible.) The well-known alternate approach of integrating the differential equation of flapping motion (ref. 4) would also have been an entirely reasonable point of departure for developing these programs.

After steady flapping and zero C_Q are attained, additional iterations are performed to attain either (a) a specified shaft angle and advance ratio by adjustment of inflow ratio λ and tip-speed ratio μ (program A), or (b) a specified resultant force at one or more shaft angles by adjustment of the jet-deflection controls (program X). When results at several angles are computed, program X proceeds in such a manner as to find the angle at which C_{jR} is minimized. Both programs assume supercritical pressure ratios and adjust jet velocity, which affects mass flow and C_{QCOR} , with each change of C_{jR} . Both programs permit suppression of arbitrary harmonics of blade flapping, so that teetering and gimbal-mounted rotors may be simulated as well as free-to-cone rotors.

A third program for shaft-driven rotors parallels program X, adjusting conventional controls to obtain a specified resultant force.

All programs include the standard assumptions of rigid blades, uniform inflow, the applicability of two-dimensional data to blade elements, small

flapping angles, no lagging motion, etc. On the other hand, effects of stall, compressibility, and spanwise section variation can be included in the two-dimensional data used.¹

Two-dimensional jet effects are accounted for in terms of the local momentum coefficient c_j (often designated c_μ), defined as $m_j V_j / q_l c$. The total section lift and drag are assumed to consist of three components each; (basic force) + (jet-reaction increment) + (supercirculation increment):

$$c_l = c_{l_0} + \Delta c_{l_j} + \Delta c_{l_s} \quad (2)$$

$$c_d = c_{d_0} + \Delta c_{d_j} + \Delta c_{d_s} \quad (3)$$

The first component of each equation is determined by table lookup and interpolation as a trivariate function of local angle of attack, Mach number, and radial station (i.e., section shape). The jet-reaction increments are obtained by geometric considerations as

$$\Delta c_{l_j} = c_j \sin(\alpha + \delta) \quad (4)$$

$$\Delta c_{d_j} = -c_j \cos(\alpha + \delta) \quad (5)$$

Based on references 5 and 6, Δc_{l_s} is calculated as

$$\Delta c_{d_s} = s_l \sqrt{c_j} \sin(\alpha + \delta) \quad (6)$$

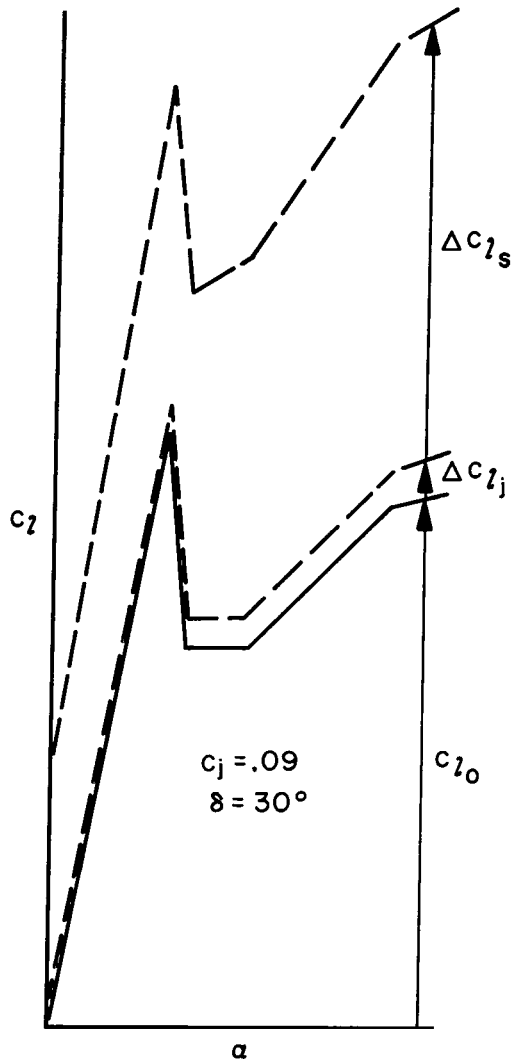
with $s_l = 3.18$ for all computations of this study (ref. 6). Finally,

$$\Delta c_{d_s} = -s_d c_j [1 - \cos(\alpha + \delta)] \quad (7)$$

with $0 \leq s_d \leq 1$. For theoretical full thrust recovery, $s_d = 1$ (i.e., $\Delta c_{d_j} + \Delta c_{d_s} = -c_j$ for all α, δ). If no thrust recovery is assumed, $s_d = 0$.

In this study, the value $s_d = 1/2$ has been used in most computations. (For a recent discussion of jet-flap thrust recovery, and a review of the literature, see reference 7, wherein it is argued that both theory and experiment indicate that full thrust recovery can be expected in steady-state flow. However, the most reasonable assumption to apply to a jet-flap rotor is not clear, and the effect of varying the parameter s_d is examined in the present study.)

¹The uniform inflow is assumed to be opposite to the direction of the resultant force rather than the thrust, resulting in an induced component v_H in the definition of μ . While the justification for this minor refinement of a gross assumption is open to question, it was found that the inclusion of v_H did not materially affect computed results.



Sketch (a)

The formulas above are applied throughout the range of angle of attack and Mach number. This approach means, among other things, that patterns of stall are not much affected by these formulas, as illustrated in sketch (a). The omission of any stall-alleviating effect may be an unduly pessimistic assumption.

The spanwise distributions of both mass flow and jet velocity have been assumed constant, which permits the definition of the rotor momentum coefficient as

$$C_{jR} = \frac{M_j V_j}{\rho (\Omega R)^2 \pi R^2}$$

where M_j is the total mass flow per second through all blades of the rotor. The relationship between local c_j and C_{jR} can be shown as

$$c_j = \frac{2C_{jR}}{\Delta x_j \sigma_x u^2}$$

Relationships among C_{jR} and pressure ratio, nozzle area, jet velocity and mass flow are based on standard thermodynamic equations with the assumption of isentropic expansion.

DESCRIPTION OF ROTORS

The jet-flap rotor analyzed in this study is two-bladed, with offset flapping hinges. The blade plan form, section variation, and twist are shown in figure 2(a). The jet flap extends from $0.7R$ to the tip. Note the rapid taper in this region from a thick section (21 percent) at the inboard end to a thin section (about 8 percent) at the tip. The thick section is required to accommodate the internal duct. Other physical parameters are: $R = 19.685$ ft, $\gamma' = 0.509$, $\eta = 0.0837$, $\sigma = 0.0488$, and nozzle height = $0.0006R$. Sign conventions for principal parameters are indicated in figure 2(b).

Figure 3 shows plots of the basic airfoil data assumed. Data for the tip section are based on curves for the NACA 64-008 section as reported in

reference 8. Data for the inboard region are based on the "Summary of Airfoil Data" (ref. 9) for NACA 6-series thick sections and on the Mach number trends suggested by comparisons of the data for the NACA 0015 and 0012 sections, as reported in references 10 and 11, respectively. Data for extreme angles of attack are based on reference 12.

A few calculations were made for a shaft-driven rotor with the same physical characteristics as the jet-flap rotor, except that airfoil data typical of the NACA 0012 section were assumed for the entire rotor blade.

RESULTS AND DISCUSSION

The material presented here is organized in three main sections. The first two sections examine the inherent characteristics of the jet-flap rotor, first at moderate speeds, and then at high speeds. The discussion in these sections is fairly lengthy because of the unfamiliar and untested nature of this type of rotor. The final section briefly compares the jet-flap rotor with conventional rotors, from the standpoint of performance capabilities and power requirements.

Characteristics of the Jet-Flap Rotor at Moderate Speeds

In this section, results for advance ratios from 0.3 to 0.5, corresponding to forward speeds from 105 to 175 knots, are examined. All results are for constant tip speed of 591 ft/sec, corresponding to $\Omega = 30$ rads/sec.

Dependence of momentum and power coefficients on shaft angle.- In figure 4(a) are shown typical curves of C_{jR} and C_p vs α_s for a fixed flight condition. The corresponding control settings and blade flapping harmonics are shown in figure 4(b). (It should be remembered that control of this rotor is accomplished exclusively by variable jet-flap deflection, the blade pitch being fixed.) For comparison, similar curves are shown in figure 5 for the shaft-driven rotor (control being conventional blade-pitch control). For the jet-flap rotor, the variation of power with shaft angle is in marked contrast to its invariance for the conventional rotor. For the latter, the classical expectation of "flapping-feathering equivalence" is clearly indicated by the results; that is, equal changes of shaft angle and longitudinal pitch control (feathering) result in an equal and opposite change of longitudinal flapping, such that the resultant force, power, and torque are unchanged. Collective pitch is essentially invariant also, whereas, for the jet-flap rotor, "collective" jet deflection \bar{A}_0 varies significantly.

This finding may be rationalized in the following way. The resultant force on the jet-flap rotor may be thought of (although it is not so calculated) as the sum of a basic rotor force and a jet-flap increment. Although the basic rotor force may be conceived of in various ways, it was calculated for purposes of illustration as the force developed by the rotor when driven entirely by an undeflected tip jet. Presented in figure 6 is the variation of the basic rotor force with shaft angle for a particular advance ratio, as well

as the incremental vectors needed to produce a specified resultant force for the jet-flap rotor. It can be seen that the incremental vector at the shaft angle for minimum C_{jR} is a compromise between minimum extension and minimum tilting of the basic force vector.

Figure 7 shows curves of C_{jR} vs α_s for advance ratios of 0.3 to 0.5 for two vehicles. (Specifically, the comparison is made for two pairs of fixed values of C_{LR} and C_X at constant rotational velocity. This corresponds to two pairs of fixed values of lift and "drag area" X/q .) Also shown in the figure is the locus of optimum shaft angles for each vehicle.

Effects of blade pitch.- While a constant blade pitch is envisioned for the jet-flap rotor, it is important to examine the effects of blade pitch for an indication of the most appropriate value to be incorporated in a practical design. Figure 8 shows the effects of various pitch angles ($\theta_{0.7}$) between 8° and 12° . It can be seen that the least power is required at 8° , and that less power would probably be required at still lower pitch angles. The collective jet deflection \bar{A}_0 increases rapidly as blade pitch is decreased from 12° (fig. 4(b)) to 8° (fig. 8(b)), as might be expected. "Longitudinal cyclic" jet deflection \bar{B}_1 decreases somewhat. In all cases, coning is virtually invariant, while all harmonics of blade flapping decrease, as the shaft angle becomes more nearly vertical.

Note that the minimum C_{jR} does not occur at the shaft angle for minimum flapping. Note also (fig. 8(c)) that the profile power coefficient C_{P_0} is very sensitive to blade pitch, whereas the power component due to Coriolis forces, $C_{P_{COR}}$, is almost invariant in the range of the results presented. The marked variation in C_{P_0} reflects marked variation in local angle of attack on the retreating blade ($\alpha_{max} = 13^\circ$ for $\theta_{0.7} = 12^\circ$). Clearly, the flight condition for these calculations is not well matched to a fixed pitch of 12° .

Effects of C_X .- In figure 9(a) are shown curves of C_{jR} vs α_s for several values of C_X . The locus of optimum values of α_s is also indicated. The power variation along this locus is shown in part (b) of the figure.

In the regime of steady forward flight for realistic machines (i.e., substantial C_X), the power increases rapidly with C_X , the principal component being the propulsive power required. Coriolis power also increases, and its importance should be noted, since it amounts to as much as one-third of the total at low C_X , and to roughly one-fourth at high C_X .

The power and momentum coefficients rise as C_X drops to zero because of a rapid rise in profile power, reflecting a rapid rise in section drag over much of the rotor. This drag rise must in turn be due to excessive local angles of attack. The process can be attributed to the high fixed pitch of the rotor blades, and the progressive rearward tilting of the tip-path plane; in a conventional rotor, the result would be increasing lift and the onset of

stall. In the jet-flap rotor, the same phenomenon occurs, so far as the "basic rotor lift" (discussed earlier) is concerned; however, the over-all lift is deliberately held constant by adjustments of the jet-flap controls.

Attainable forces.- In figure 9, results were presented for the jet-flap rotor for propulsive force coefficients up to $C_X = 0.015$ at an advance ratio of 0.5. For the same conditions, it is shown in figure 10 that, at the highest C_X , the maximum jet deflection ($\bar{A}_0 + |\bar{B}_1|$) exceeds 70° for the shaft angles computed. At this highest C_X , the effect of varying C_{LR} (choosing the optimum shaft angle for each case) is shown in figure 11. It can be seen that both C_{jR} and δ_{max} are minimized at $C_{LR} \approx 0.006$ ($C_{LR}/\sigma = 0.123$). The value of δ_{max} at this condition is about 72° . The values $C_{LR} = 0.006$, $C_X = 0.015$, and $V/\Omega R = 0.5$ correspond, respectively, to $L = 6060$ lb, $X/q = 18.25$ ft², and $V = 175$ knots, and suggest the order of magnitude of attainable forces at this moderately high forward speed. Similar data for one-half the propulsive force are also shown in the figure, where it can be seen that C_{jR} and δ_{max} are minimized at $C_{LR} \approx 0.005$ ($C_{LR}/\sigma = 0.102$).

Effects of nozzle area.- A given value of C_{jR} may be the result of varying combinations of mass flow and jet velocity ($C_{jR} = C_{mass} \times (V_j/\Omega R)$). While this does not affect local section forces, which are dependent only on local c_j without regard to its component factors, it does affect Coriolis forces, which are dependent on radial mass flow. Therefore, C_{PCOR} might be sensitive to the parameter affecting mass flow in these computations, namely, the area of the nozzle. However, the results of a comparison of two nozzle areas, shown in figure 12, indicate only a slight effect. (The comparison is made for the same flight condition, not the same C_{jR} . The larger nozzle area is some 14 percent greater than the smaller, which was the value used for all other computations of this study.)

This minor effect of A_N on C_{PCOR} is partly attributable to the fact that C_{PCOR} can be shown to be roughly proportional to $\sqrt{A_N}$ rather than to A_N itself, for constant C_{jR} . However, because of differences in jet density, the actual effect in the results of figure 12 is even less than would be indicated by this approximate relationship.

Effects of higher harmonic control.- Possible benefits of higher harmonic control of the jet flap were briefly investigated. It was found that the cosine and sine components of the second harmonic of blade flapping could be almost independently suppressed by the corresponding components of second harmonic jet-flap deflection (\bar{B}_2 and \bar{A}_2 , respectively), at least for the arbitrary flight condition chosen ($V/\Omega R = 0.3$, $\alpha_s = -18.46^\circ$, $\bar{A}_0 = -20.566^\circ$, $\bar{A}_1 = 0$, $\bar{B}_1 = 12.577^\circ$, resulting in $C_{LR} = 0.0048$ and $C_X = 0.0112$). The effects of such second harmonic control on the distributions of β , C_T , and C_Q are shown in figure 13. The principal effect is a drastic reduction in the second harmonic of C_T , but some reduction is also effected in the third harmonic,

and in both the second and third harmonics of C_Q . The first harmonics of both C_T and C_Q are slightly increased. To the extent that shake and vibrations are due to higher harmonics of force and moment variations, these results strongly suggest the potential reduction of such undesirable effects through appropriate use of higher harmonic control.

Characteristics of the Jet-Flap Rotor at High Speeds

In this section, results for advance ratios from 0.50 to 0.86, corresponding to forward speeds from 175 to 301 knots, are examined.

Results at constant ΩR .- Results obtained at high advance ratios are shown in figure 14. The lift and propulsive force coefficients are the same as for certain data of figure 9, and correspond to fixed values of vehicle weight and drag area of 4920 lb and 6.09 sq ft, respectively. The highest advance ratio shown, 0.86, corresponds to a flight velocity of 301 knots, a speed at which pure helicopter flight would not be computable under any reasonable assumptions, for any conventional rotor. At this extreme condition, the advancing tip Mach number is 0.98, which, though high, is not necessarily impractical, in view of the thin tip section. At both this advance ratio and the advance ratio of 0.8, a portion of the jet flap encounters the region of reverse flow on the retreating blade.

Other than the high flight velocity of 301 knots, the results presented involve no particular surprises. The variations of C_{jR} with α_s are entirely similar to those at lower advance ratios. The jet-deflection requirements increase with advance ratio, but at a decreasing rate. Power requirements build up rapidly, particularly the propulsive power required, which increases as the cube of advance ratio (for constant C_X). Compressibility effects are reflected in increasing C_{P_0} and momentum requirements in $C_{P_{COR}}$.

Again, the significant finding would seem to be the mere fact that it was possible to compute a 300-knot case for positive propulsive force and significant lift.

Results at limited tip Mach number.- If advancing tip Mach number is to be restricted to avoid severe compressibility effects, it is necessary to reduce rotational velocity as advance ratio is increased beyond some particular value. To examine this mode of high-speed flight, results were obtained at an advance ratio of 0.7 and an advancing tip Mach number of 0.8, the same as that which prevailed at an advance ratio of 0.5 in the results previously discussed. The forward speed corresponding to these conditions was 220 knots, and the tip speed, ΩR , was 531 ft/sec, corresponding to $\Omega = 27$ rads/sec.

Results are presented in figure 15 for two values of C_X , corresponding to drag areas of 6.09 and 9.13 sq ft. As in the earlier high-speed results, the lift was 4920 lb, but the coefficient C_{LR} was necessarily higher because of the reduction in Ω .

Some power saving was realized, in both the Coriolis and profile power components. These savings (not illustrated) amounted to about 20 percent and 15 percent, respectively, for the lower C_X . The largest component, propulsive

power, was necessarily the same. (The power components were compared on a dimensional basis at the same forward speed.)

An adverse effect can be seen in the increase in required jet deflection. As a specific example, at the optimum shaft angles, δ_{max} for $C_X = 0.005$ at $V = 220$ knots (fig. 15) was greater than for the same C_X at $V = 245$ knots (fig. 14). Primarily because of this effect of rapidly increasing δ_{max} with forward speed, no attempt was made to compute higher speed cases for an advancing tip Mach number of 0.8. It may be worth noting that such flight at 300 knots would require an advance ratio of 1.3, and an increase of 53 percent in C_{LR} .

Effects of the thrust recovery parameter.- One-half of the theoretical full thrust recovery due to supercirculation has been assumed in the calculations discussed so far; that is, the parameter s_d has been set equal to one-half in equation (7). In view of the large jet deflections in the high-speed results just discussed, it was felt that the effects of varying s_d for one of these cases would be particularly illuminating. This has been done for the full range of s_d , from 0 to 1, for the least-propulsive-force flight condition of figure 15 ($C_X = 0.005$), and results are shown in figure 16. Although C_{jR} decreases with increasing s_d , as would be expected, the variation is not large. More importantly, the required maximum flap deflections increase rapidly; for example, at $\alpha_s = -16^\circ$, δ_{max} increases from 69° without thrust recovery to 109° with full thrust recovery. Cross plots of δ_{max} against s_d suggest that there probably exist conditions (of greater speed, or greater propulsive force) for which a solution could be computed for $s_d = 0$, but could not be computed for $s_d = 1$. In short, the results seem almost paradoxical in that they suggest that high-speed flight is more readily attainable if less thrust recovery actually occurs in a real machine.

Another approach to examining the effects of assumed thrust recovery is to consider the variation of rotor forces with s_d for fixed control settings and shaft angle. This has been done and results are shown in figure 17. It can be seen that, relative to the usual value of $s_d = 1/2$, the value of C_X is doubled for $s_d = 0$, and cut in half for $s_d = 1$. The corresponding range of disk tilt ($\alpha_s + a_1$) is about 5° . Again, the result seems paradoxical until the variation of C_{jR} is considered; the greater force without thrust recovery is simply due to much greater momentum flux required to turn the rotor, and the lesser force with full thrust recovery is due to the fact that the rotor turns with much lower momentum flux by virtue of the thrust recovery assumed.

The general conclusion may be drawn at this point that speeds well in excess of 200 knots may be attainable for practical pure helicopters with jet-flap rotors, particularly if little or no supercirculatory thrust recovery occurs on the rotor blades in practice.

Comparisons With Conventional Rotors

The comparisons in this section are concerned with performance capabilities and power requirements.

High performance characteristics.- From the generalized charts of reference 13, one may draw certain conclusions as to the attainable flight conditions for conventional shaft-driven rotors. (The charts are based on digital computations which are considered comparable to those of the present study.) For example, a solidity of about 0.11 for rectangular blades with -8° of twist would be required to attain the flight condition of $C_{LR} = 0.00488$, $C_X = 0.0113$, and $V/\Omega R = 0.5$ (corresponding to the results presented on figures 7 and 9 for the jet flap rotor). This solidity is greater than that of the jet-flap rotor by a factor of about 2.2, and the required machine can be visualized as a 4-bladed rotor with blades of about 10 percent greater effective chord. To attain the greater resultant force of $C_{LR} = 0.0065$, $C_X = 0.015$ (fig. 7) would require an approximate threefold increase in solidity to about 0.15.

On the basis of the charts, the maximum attainable design speed of a conventional pure helicopter can be estimated to be about 200 knots or slightly more. The solidity required for such speeds would be more than three times that of the jet-flap rotor. A few current design studies, such as references 14 and 15, likewise indicate a speed limit of this order, regardless of solidity or any other design parameter. In contrast, as has already been shown, computational results can be obtained for the jet-flap rotor for speeds as high as 300 knots.

Specific power comparison.- A few computations were carried out for a shaft-driven rotor having the same physical characteristics as the jet-flap rotor, except that airfoil data based on the characteristics of the NACA 0012 section were applied to the entire blade. It may be instructive to compare this rotor with the jet-flap rotor for the same specific flight condition. This has been done in figure 18 for the condition of $C_{LR} = 0.00488$, $C_X = 0.0113$, and $V/\Omega R = 0.3$, for which jet-flap results were presented in figure 7(b), and for which the conventional rotor is close to stall. The jet-flap rotor clearly requires more power. While the data of figure 8(c) suggest that substantial reductions in C_{P_0} might be obtained through an optimum choice of blade pitch θ , they also indicate that significant reductions in $C_{P_{COR}}$ are probably not attainable. Since $C_{P_{COR}}$ for the jet-flap rotor is significantly higher than C_{P_0} for the shaft-driven rotor, it appears that total power required for the former would generally, and perhaps always, be higher than that required for the latter, for the same flight condition. However, while the conventional rotor is close to stall at this condition, the jet-flap rotor can generate far greater forces, and far greater speeds, as has already been shown.

CONCLUSIONS

Under the assumptions made, this study has led to the following conclusions:

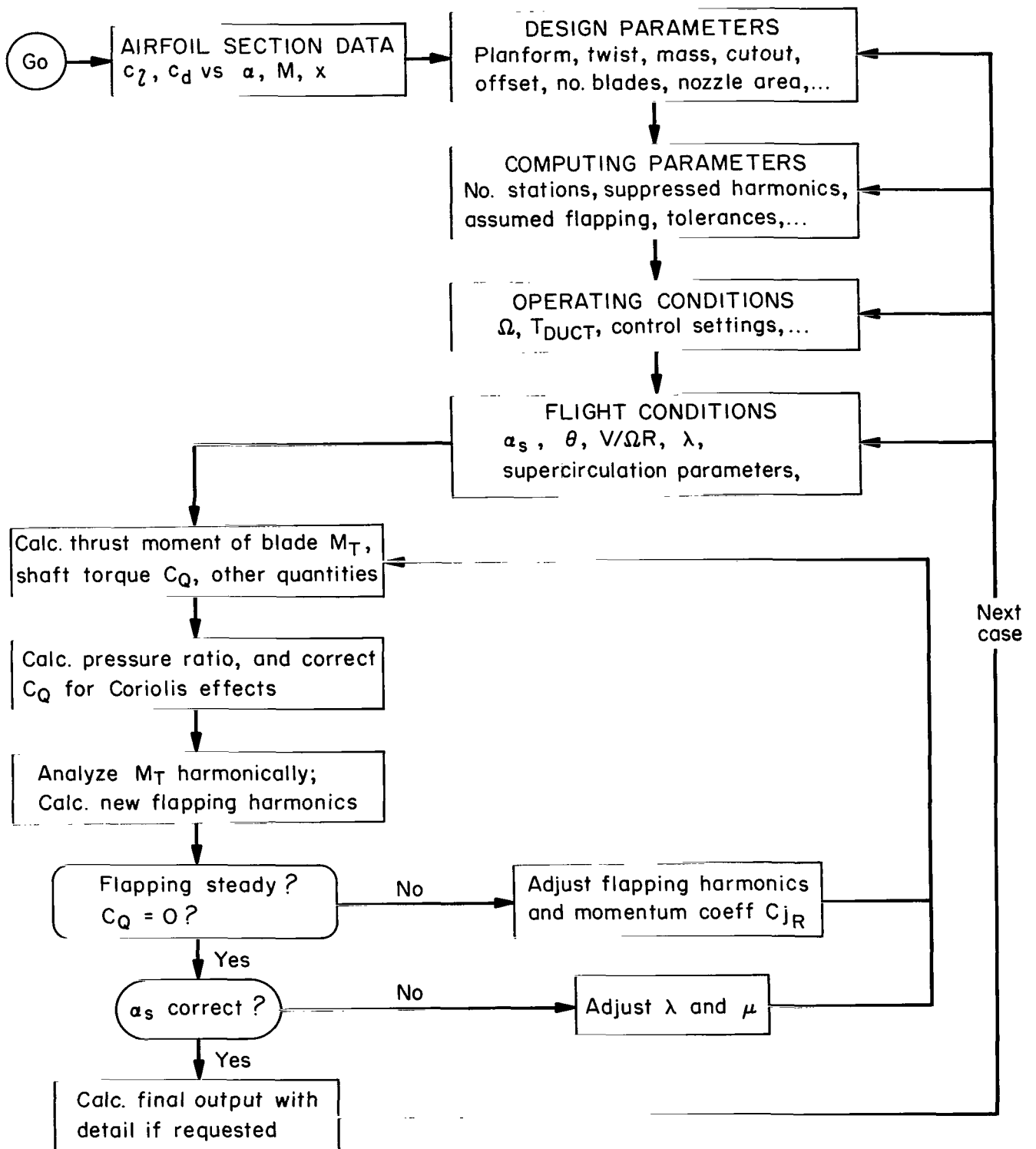
1. A jet-flap rotor appears capable of higher self-propelled speed than any conventional rotor.
2. A jet-flap rotor can generate far greater forces than a conventional rotor of the same radius and solidity.
3. For unstalled flight conditions, a jet-flap rotor requires more power than a conventional rotor of basically similar design.
4. The maximum attainable speed of a jet-flap rotor is likely to be higher if theoretical supercirculatory thrust recovery on the blade is not realized in practice.
5. The momentum and power coefficients required for a given flight condition vary significantly with shaft angle.
6. Higher harmonic control of the jet flap is likely to reduce vibrations.
7. The nozzle height does not appear to be a sensitive parameter in jet-flap rotor design.

Ames Research Center
National Aeronautics and Space Administration
Moffett Field, Calif., July 21, 1965

REFERENCES

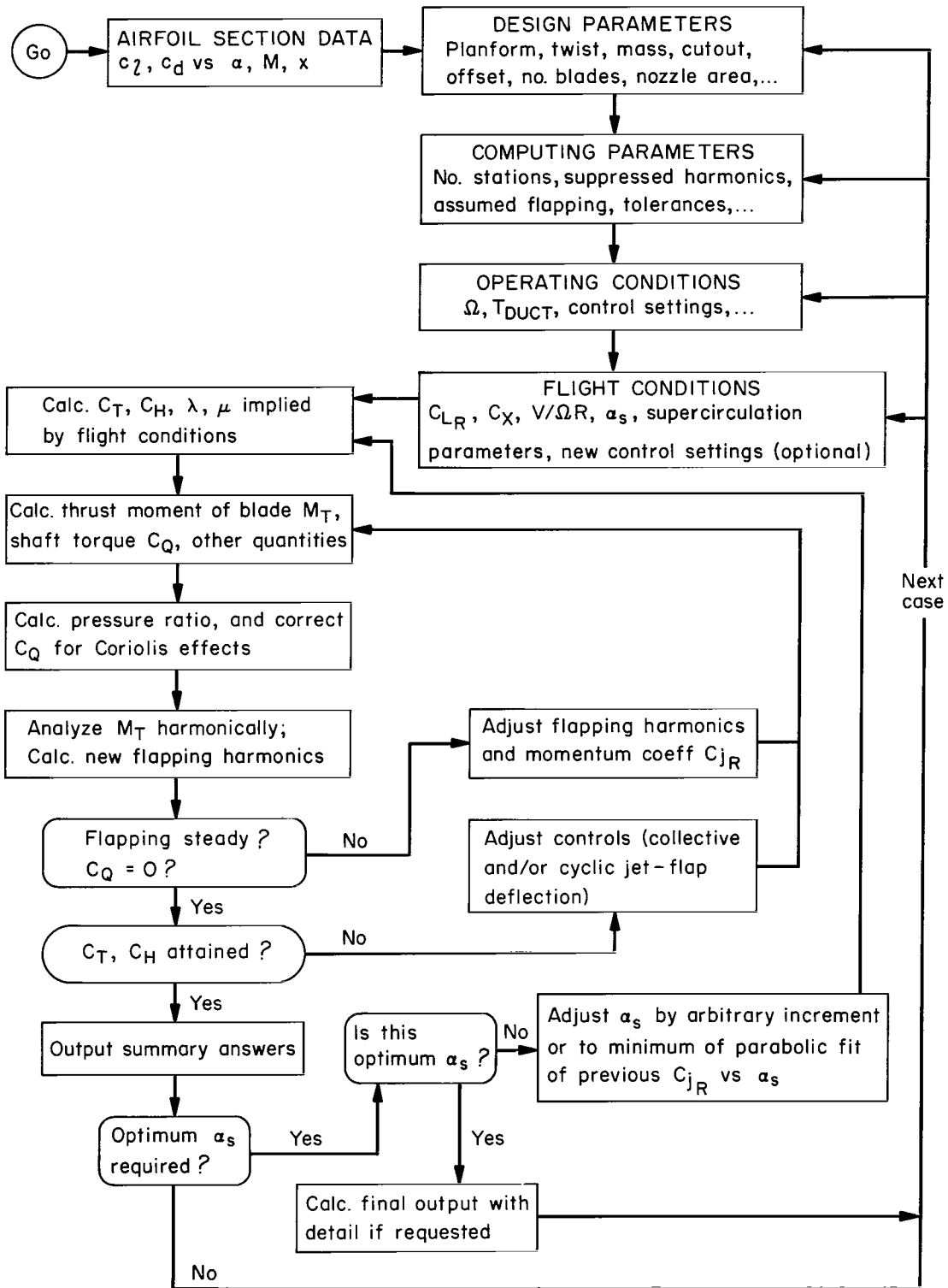
1. Dorand, René; and Boehler, Gabriel D.: Application of the Jet-Flap Principle to Helicopters. J. Am. Helicopter Soc., v. 4, no. 3, July 1959, pp. 26-36.
2. Greeman, R. N.; and Gaffney, M. G.: Application of Circulation Control to Helicopter Rotors. Rep. ARD 158, Hiller Helicopter Co., 1957.
3. Gessow, Alfred: Equations and Procedures for Numerically Calculating the Aerodynamic Characteristics of Lifting Rotors. NACA TN 3747, 1956.
4. Gessow, Alfred; and Crim, Almer D.: A Method for Studying the Transient Blade-Flapping Behavior of Lifting Rotors at Extreme Operating Conditions. NACA TN 3366, 1955.

5. Malavard, L.; Jousserandot, P.; and Poisson-Quinton, Ph.: Jet-Induced Circulation Control. *Aero Digest*, vol. 73, nos. 3-5, 1956: Sept., pp. 21-27; Oct., pp. 46-59; Nov., pp. 34-46.
6. Dike, D. J.; Dunn, H. S.; Hazen, D. C.; and Lehnert, R. F.: A Study of the Low Speed Aerodynamic Characteristics of High-Lift Flow Controlled Profiles and Wings. *Aeron. Engr. Rep. 349*, Princeton Univ., 1958.
7. Garland, D. B.: Jet-Flap Thrust Recovery: Its History and Experimental Realisation. *AIAA Paper 64-797*, 1964.
8. Wilson, Homer B., Jr.; and Horton, Elmer A.: Aerodynamic Characteristics at High and Low Subsonic Mach Numbers of Four NACA 6-Series Airfoil Sections at Angles of Attack From -2° to 31° . *NACA RM L53C20*, 1953.
9. Abbott, Ira H.; von Doenhoff, Albert E.; and Stivers, Louis S., Jr.: Summary of Airfoil Data. *NACA TR 824*, 1945.
10. Shivers, James P.; and Carpenter, Paul J.: Effects of Compressibility on Rotor Hovering Performance and Synthesized Blade-Section Characteristics Derived From Measured Rotor Performance of Blades Having NACA 0015 Airfoil Tip Sections. *NACA TN 4356*, 1958.
11. Carpenter, Paul J.: Lift and Profile-Drag Characteristics of an NACA 0012 Airfoil Section as Derived From Measured Helicopter-Rotor Hovering Performance. *NACA TN 4357*, 1958.
12. Critzos, Chris C.; Heyson, Harry H.; and Boswinkle, Robert W., Jr.: Aerodynamic Characteristics of NACA 0012 Airfoil Section at Angles of Attack From 0° to 180° . *NACA TN 3361*, 1955.
13. Tanner, Watson H.: Charts for Estimating Rotary Wing Performance in Hover and at High Forward Speeds. *NASA CR-114*, 1964.
14. Tanner, Watson H.; and Bergquist, Russell R.: Some Problems of Design and Operation of a 250-Knot Compound Helicopter Rotor. *J. Aircraft*, vol. 1, no. 5, Sept.-Oct. 1964, pp. 252-259.
15. Wachs, Miller A.; and Rabbott, John P., Jr.: Rotary Wing Aircraft Design Trends. Paper presented at Vehicle Design and Propulsion Meeting, Wright-Patterson AFB, Ohio, Sikorsky Aircraft, 1963.



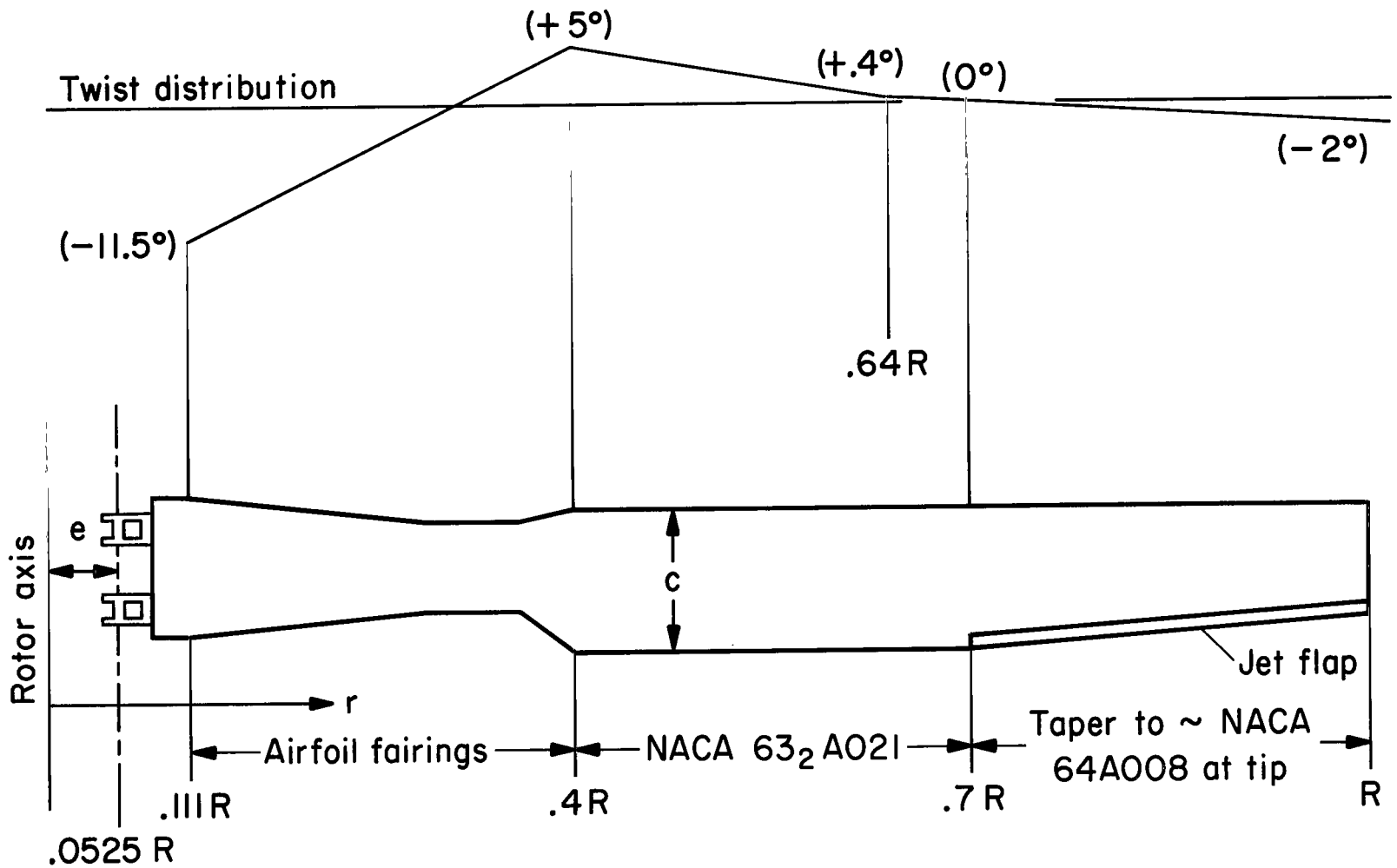
(a) Flow chart for program A.

Figure 1.- Flow charts for the computing programs for the jet-flap rotor.



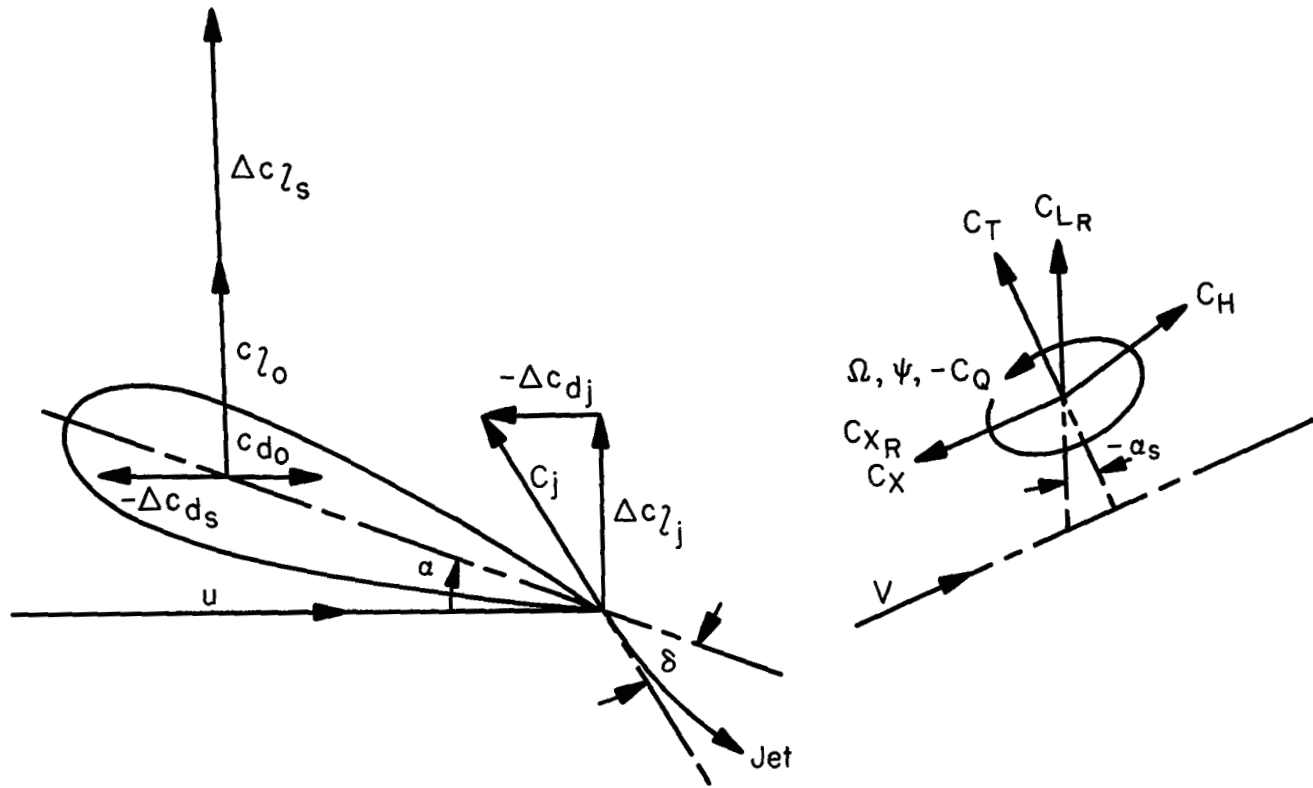
(b) Flow chart for program X.

Figure 1.- Concluded.



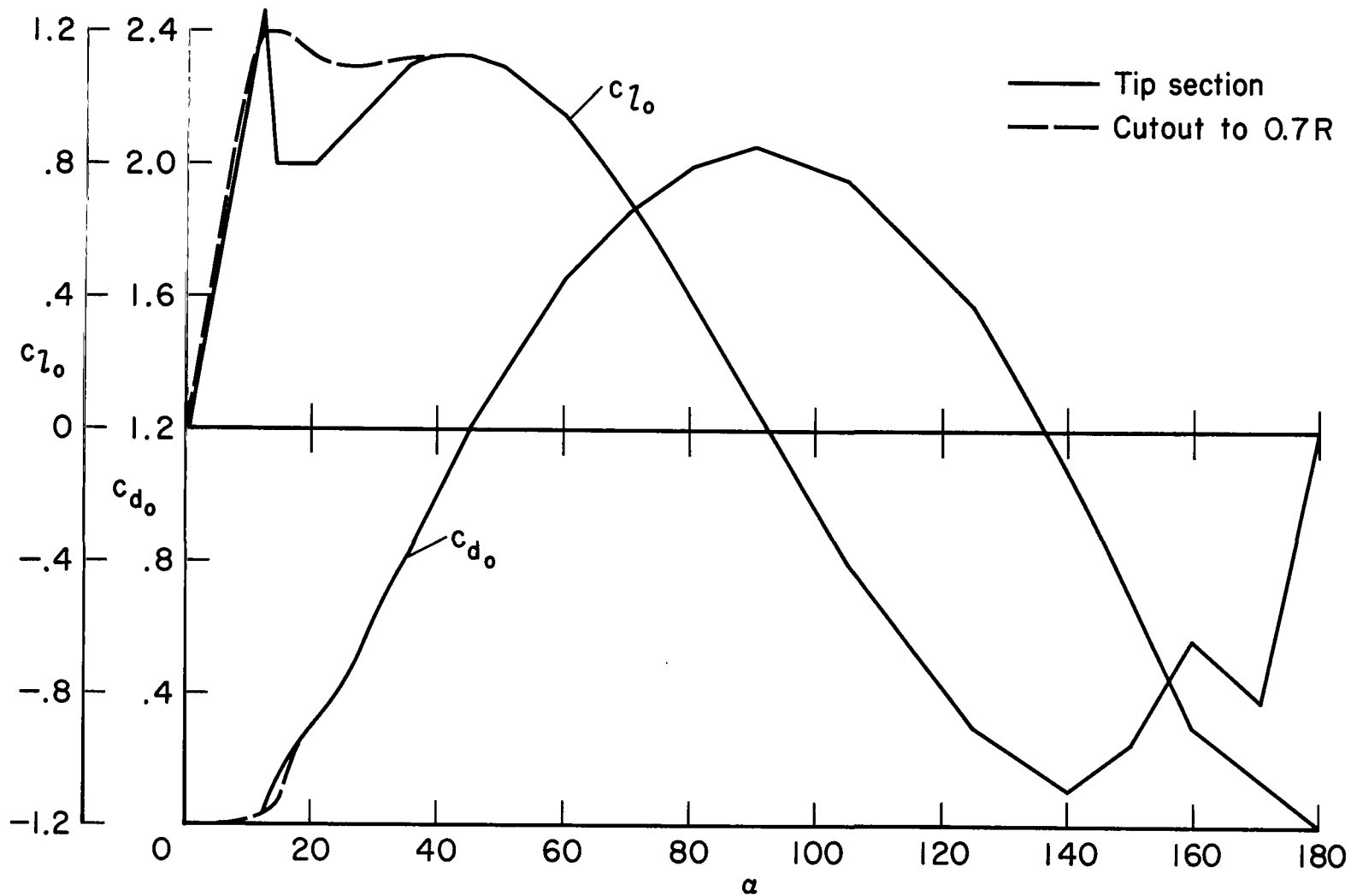
(a) Plan form, section variation, and twist of blade.

Figure 2.- Rotor details.



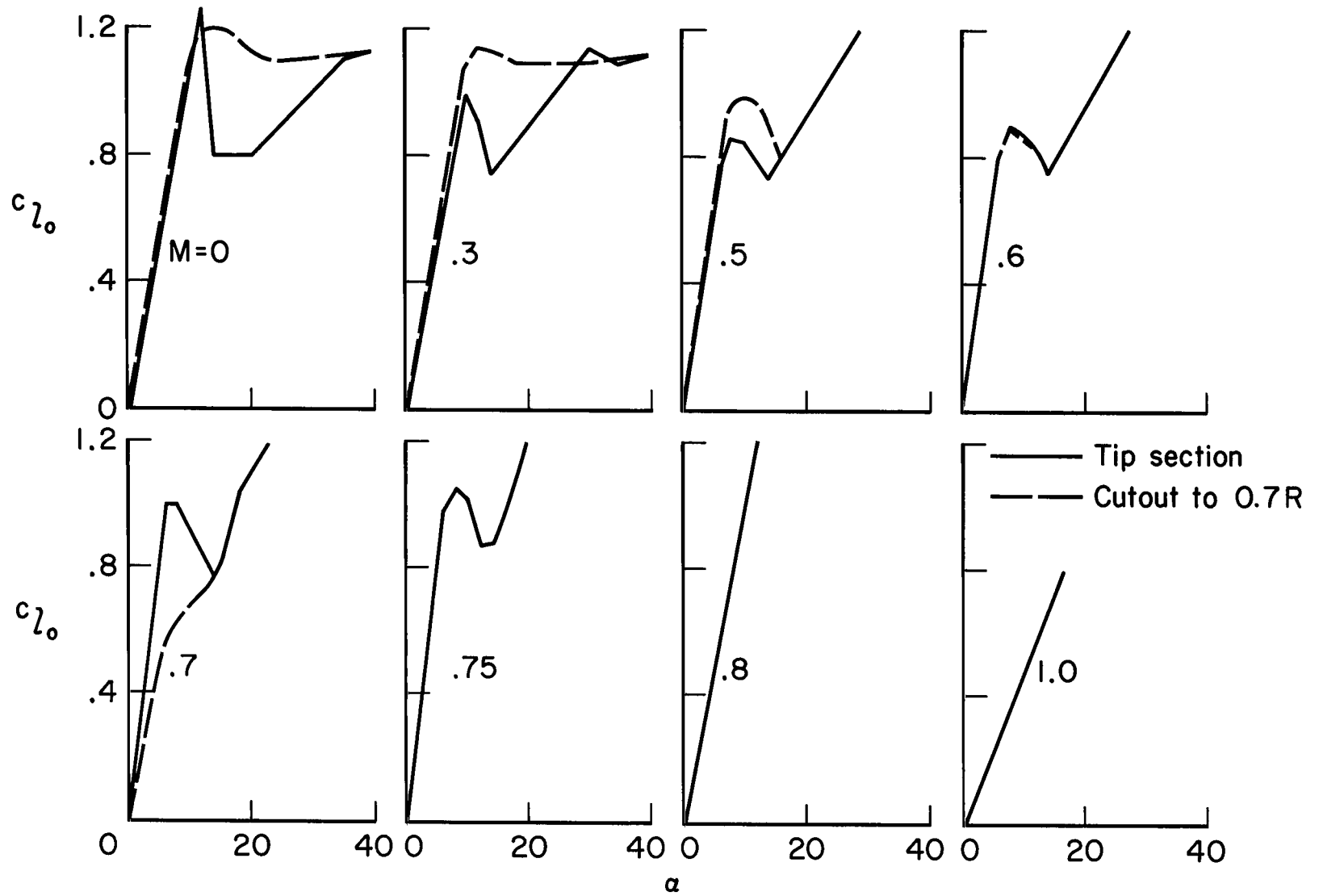
(b) Sign conventions for principal parameters.

Figure 2.- Concluded.



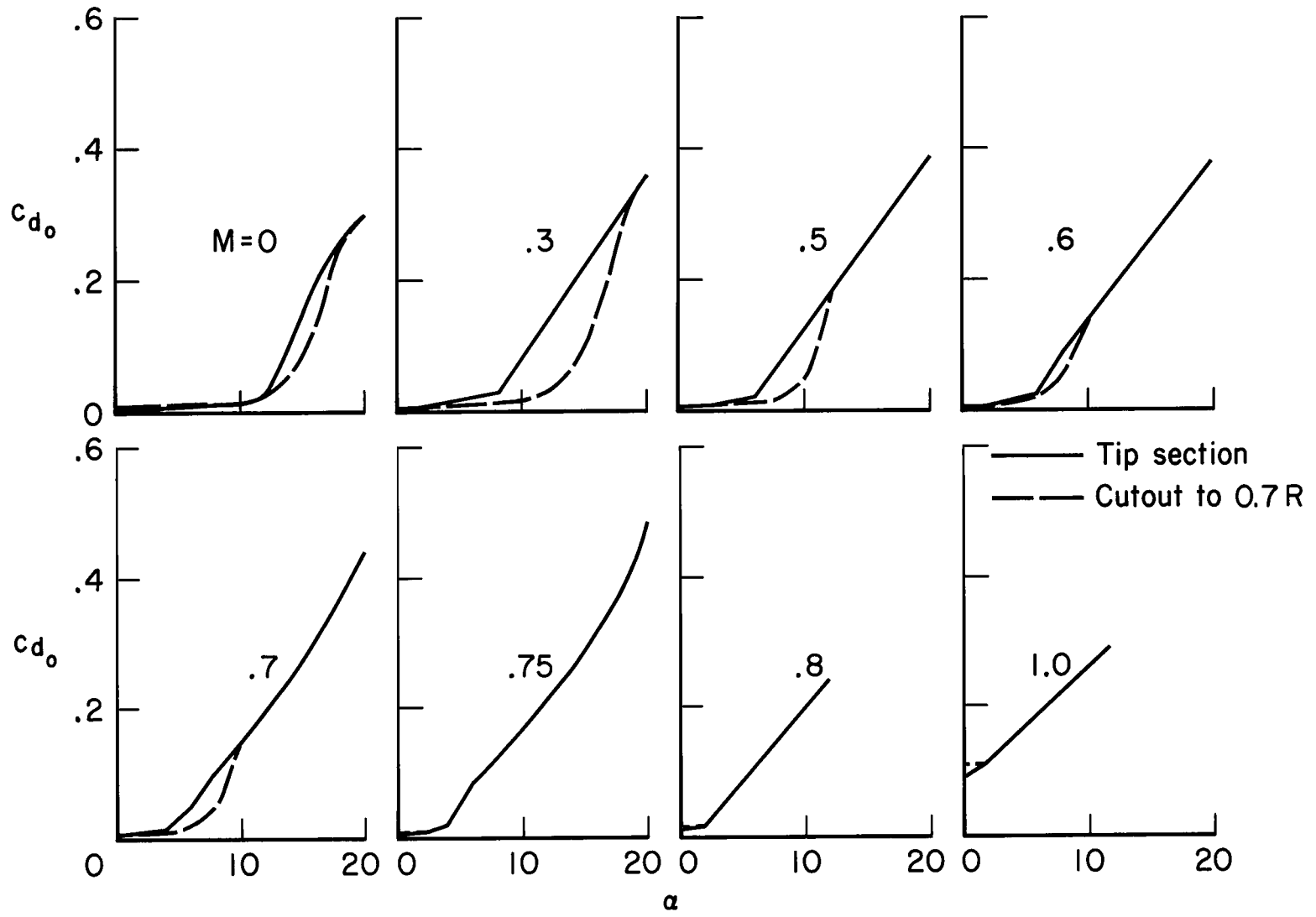
(a) Data through 180° at zero Mach number.

Figure 3.- Basic blade-section data.



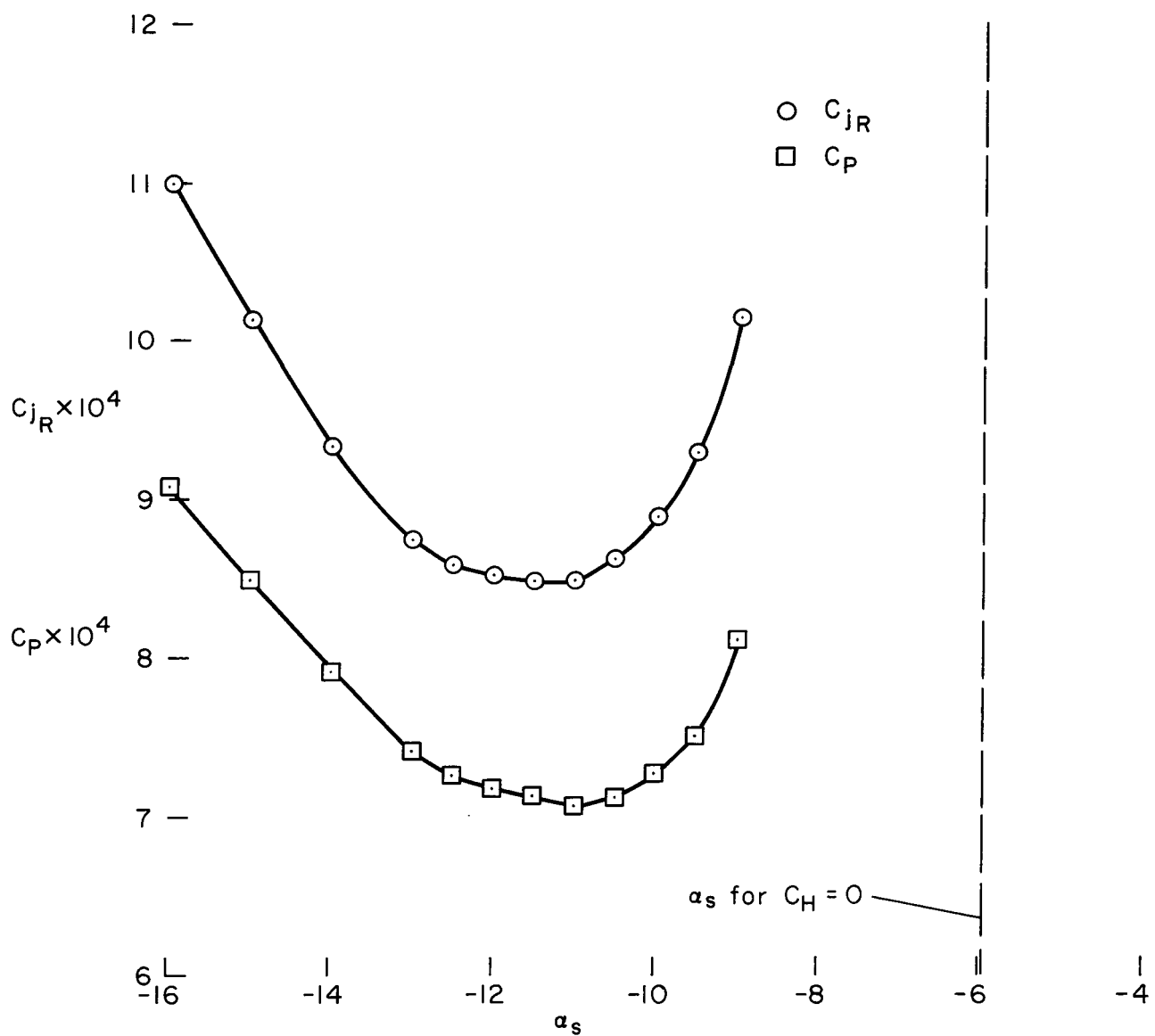
(b) Lift data.

Figure 3.- Continued.



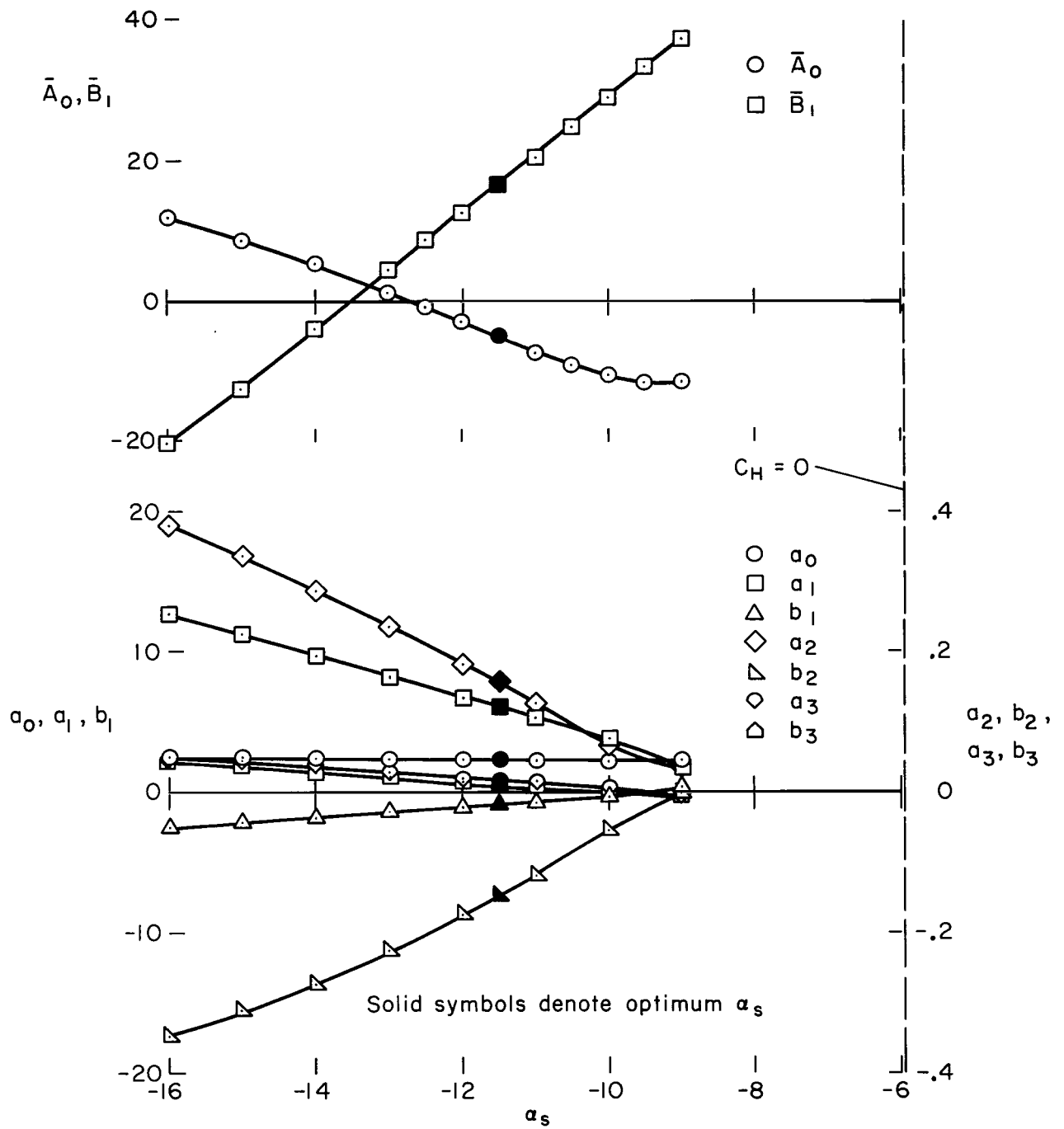
(c) Drag data.

Figure 3.- Concluded.



(a) Effects on C_{jR} and C_P .

Figure 4.- Effects of shaft angle at a fixed flight condition for the jet-flap rotor; $C_{LR} = 0.0065$, $C_X = 0.015$, $V/\Omega R = 0.3$, $\theta_{0.7} = 12^\circ$, $\Omega R = 591$ ft/sec.



(b) Effects on control requirements and blade flapping.

Figure 4.- Concluded.

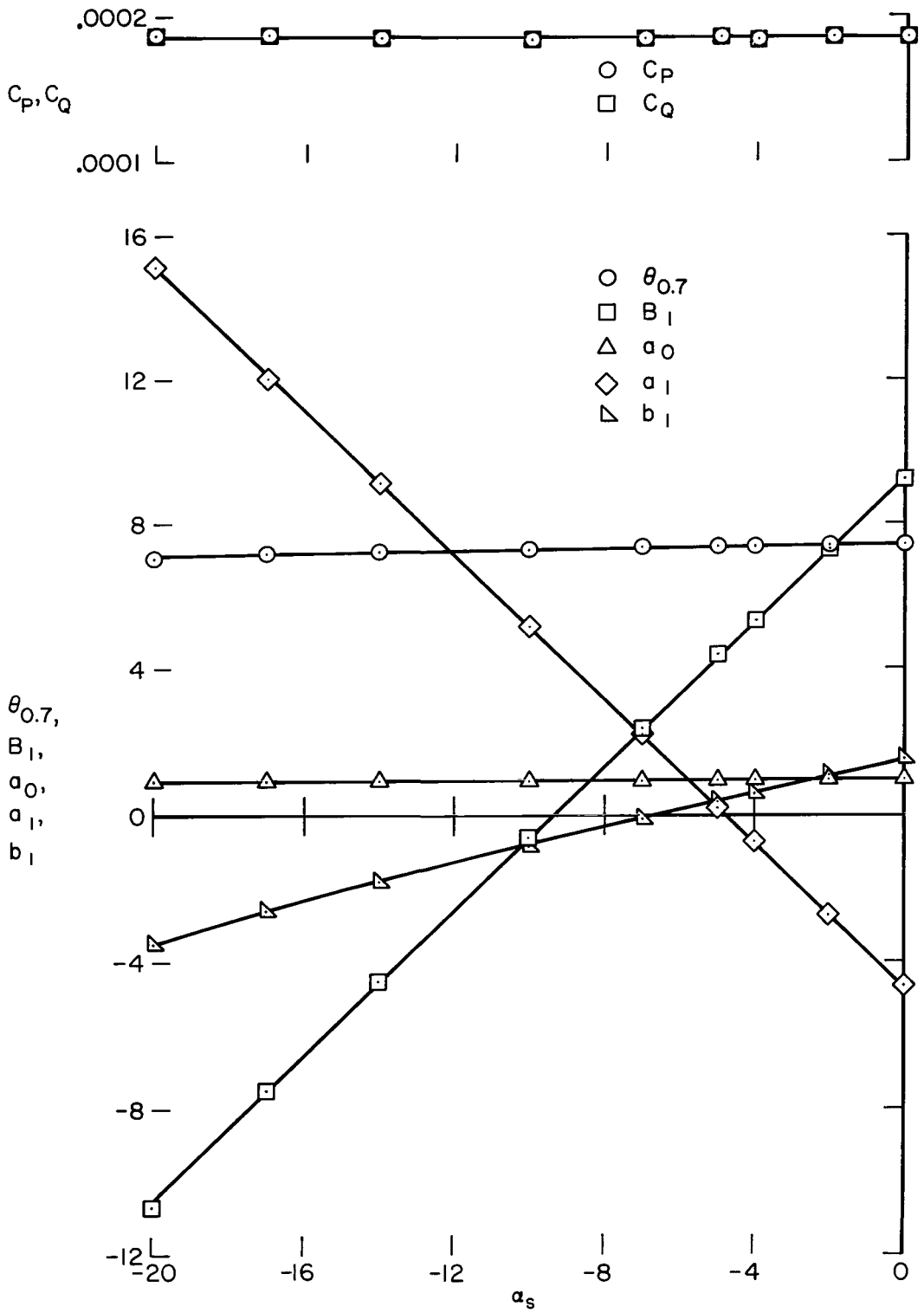


Figure 5.- Effects of shaft angle at a fixed flight condition for the shaft-driven rotor; $C_{LR} = 0.003$, $C_X = 0.005$, $V/\Omega R = 0.3$, $\Omega R = 591$ ft/sec.

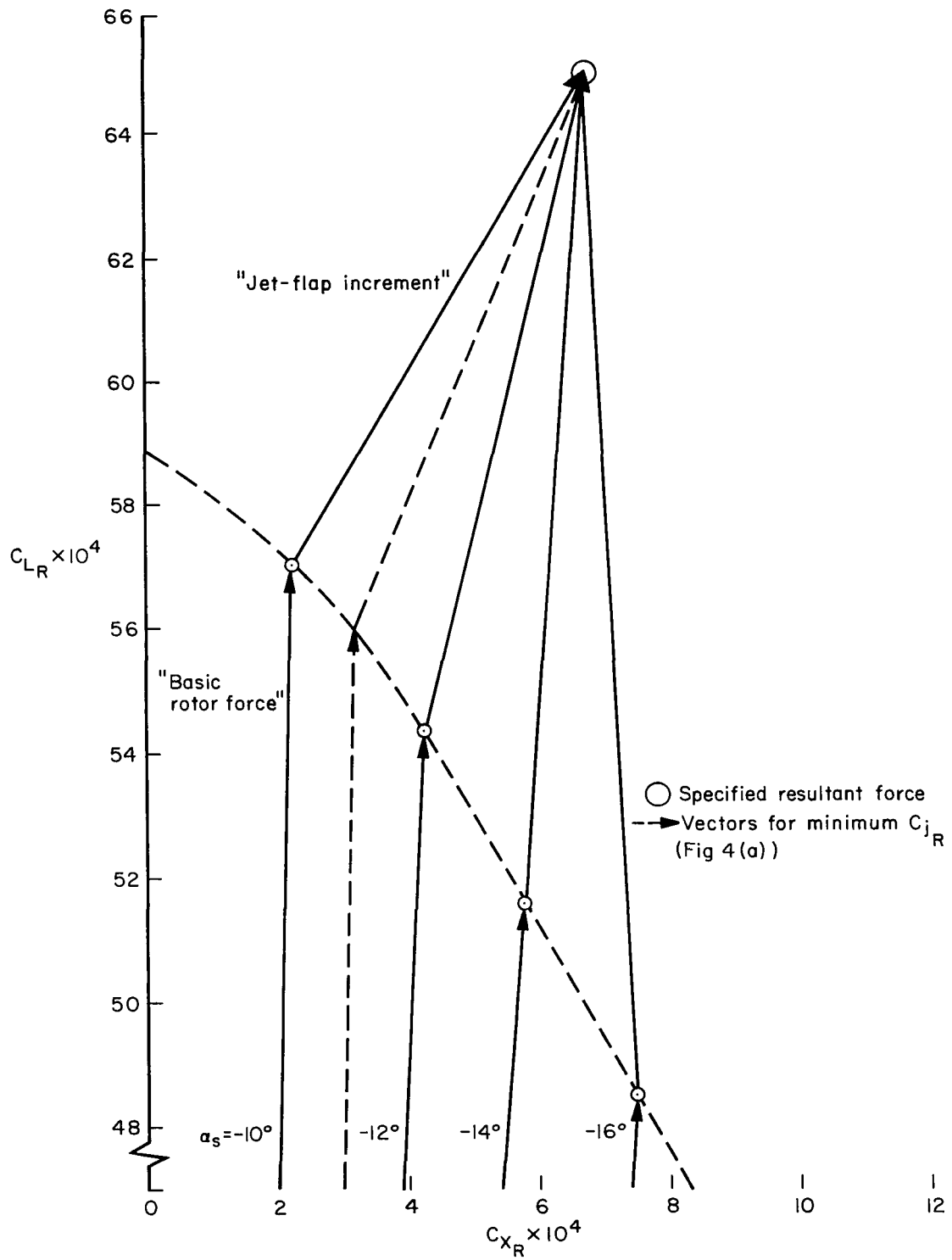
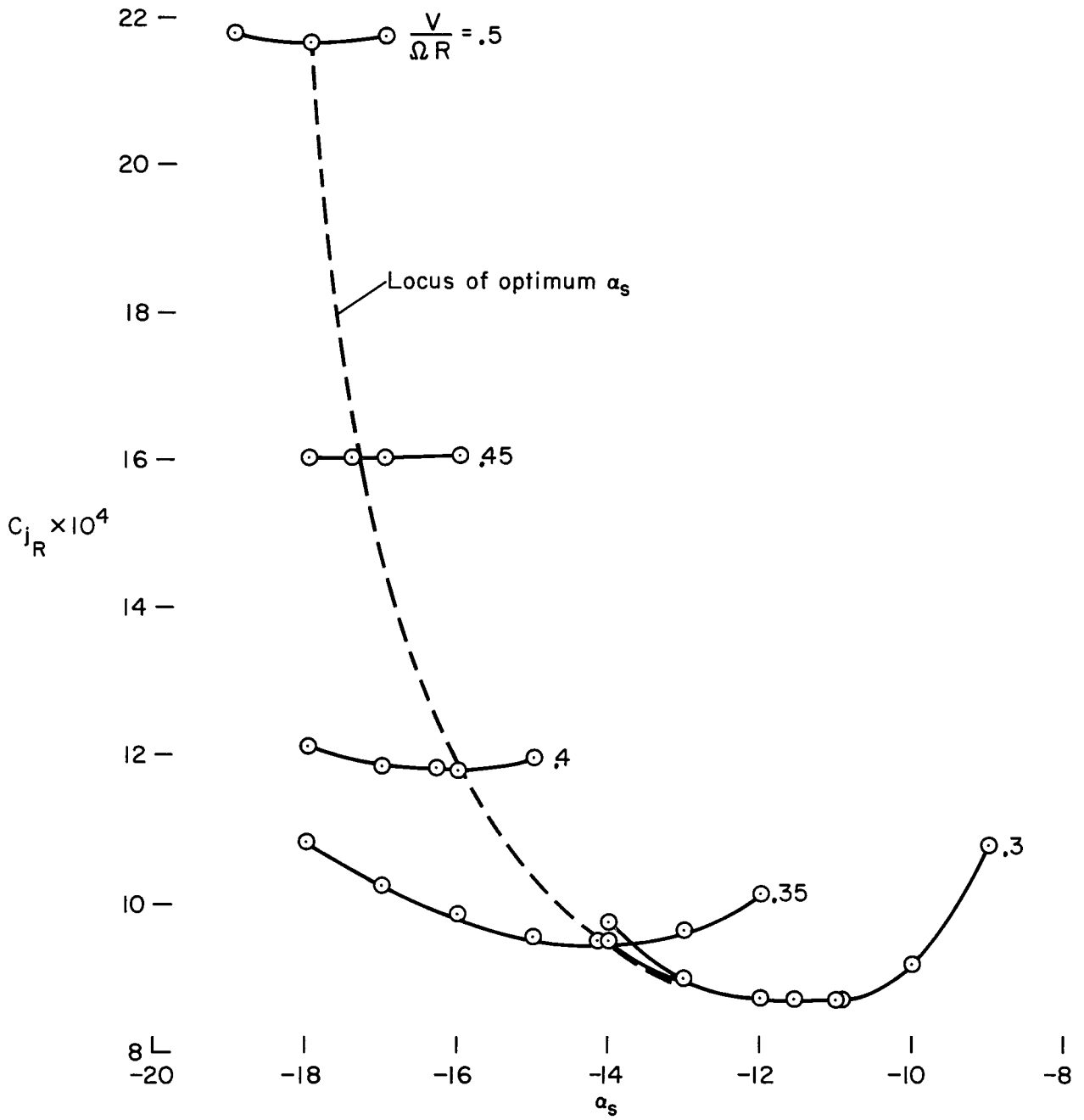
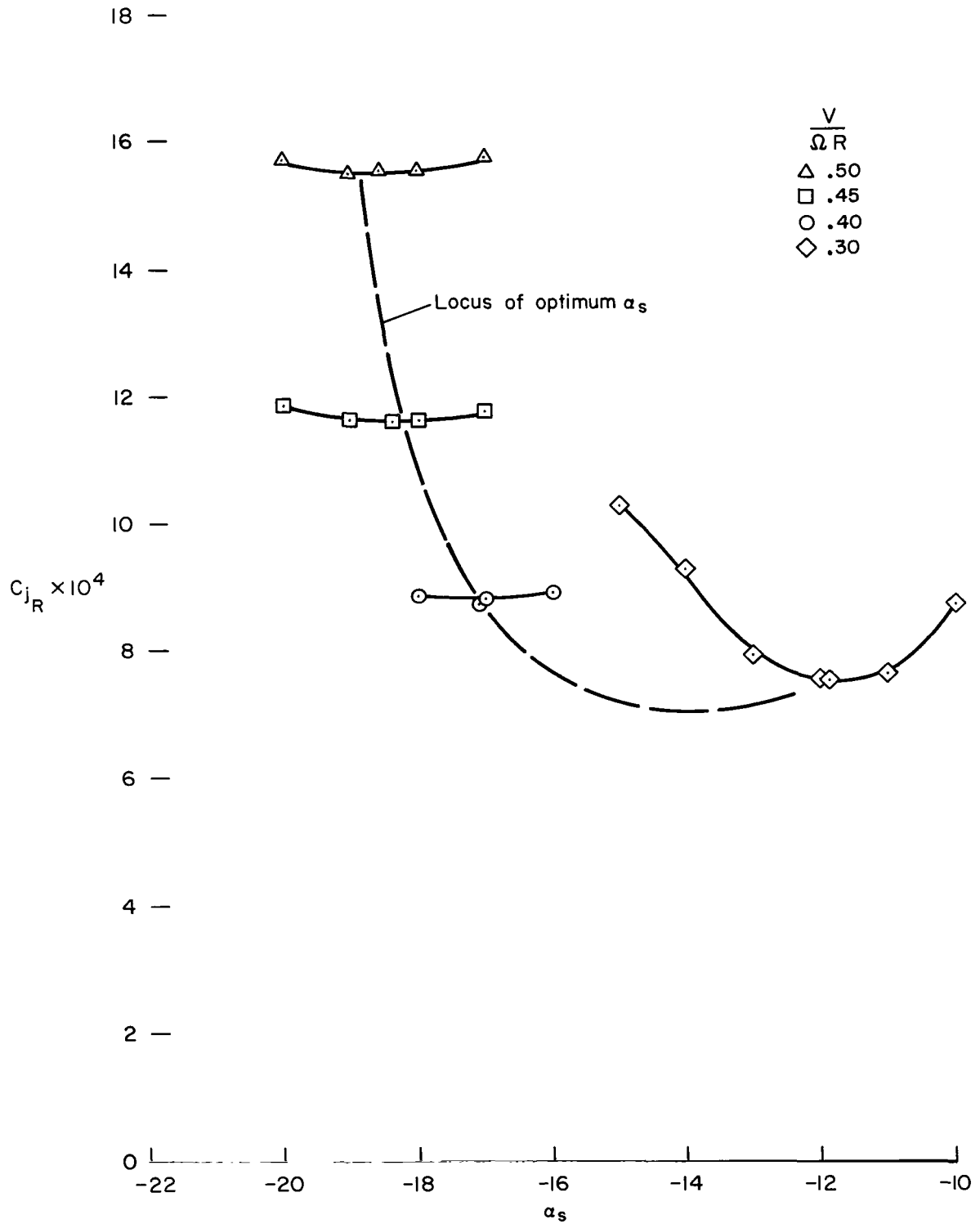


Figure 6.- Basic and incremental forces for the jet-flap rotor at various shaft angles; $V/\Omega R = 0.3$, $\Omega R = 591$ ft/sec.



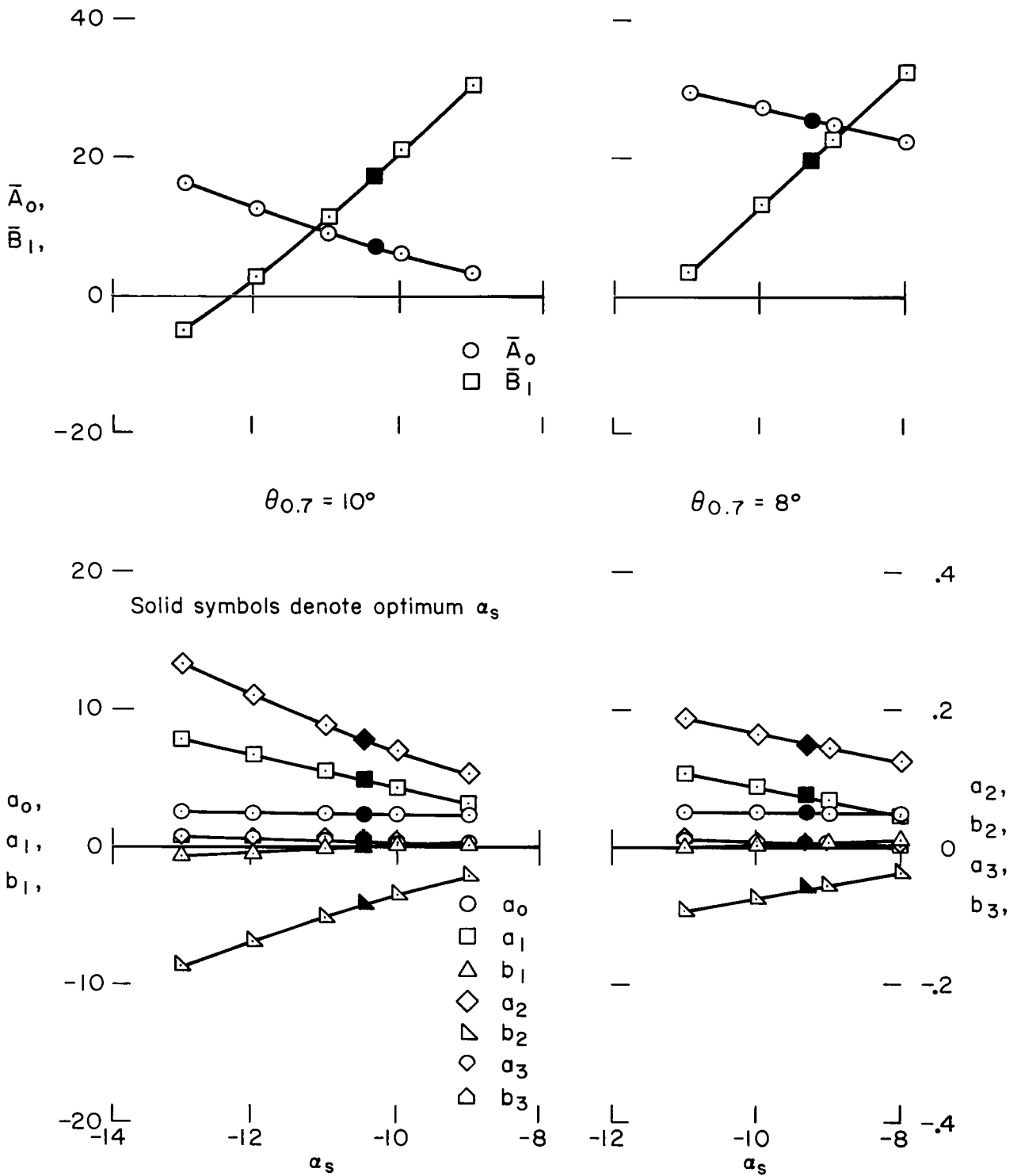
(a) $C_{LR} = 0.0065$, $C_X = 0.015$

Figure 7.- Variation of optimum shaft angle with advance ratio for the jet-flap rotor; $\theta_{0.7} = 12^\circ$, $\Omega R = 591$ ft/sec.



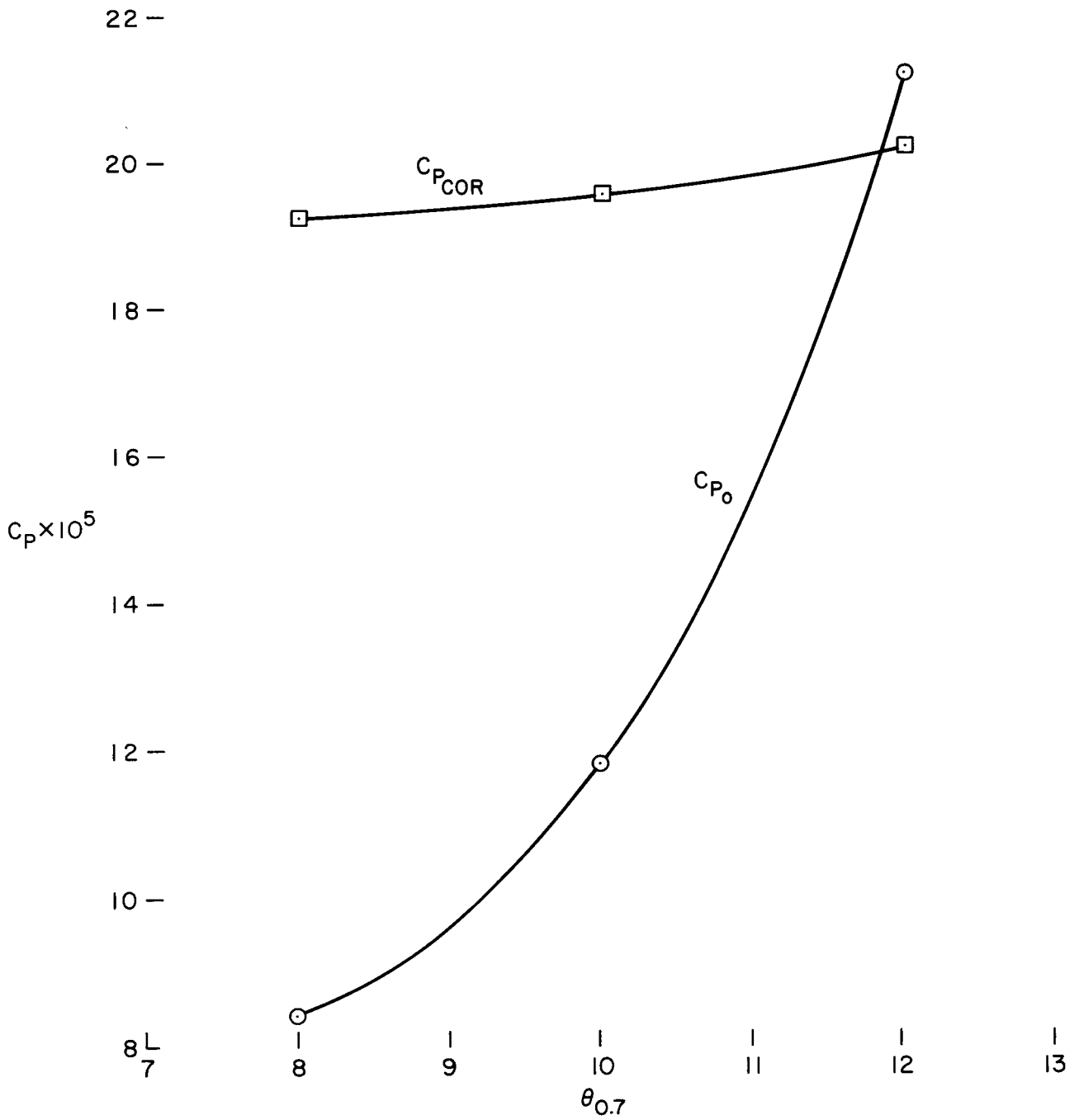
(b) $C_{I_R} = 0.00488$, $C_X = 0.0113$

Figure 7.- Concluded.



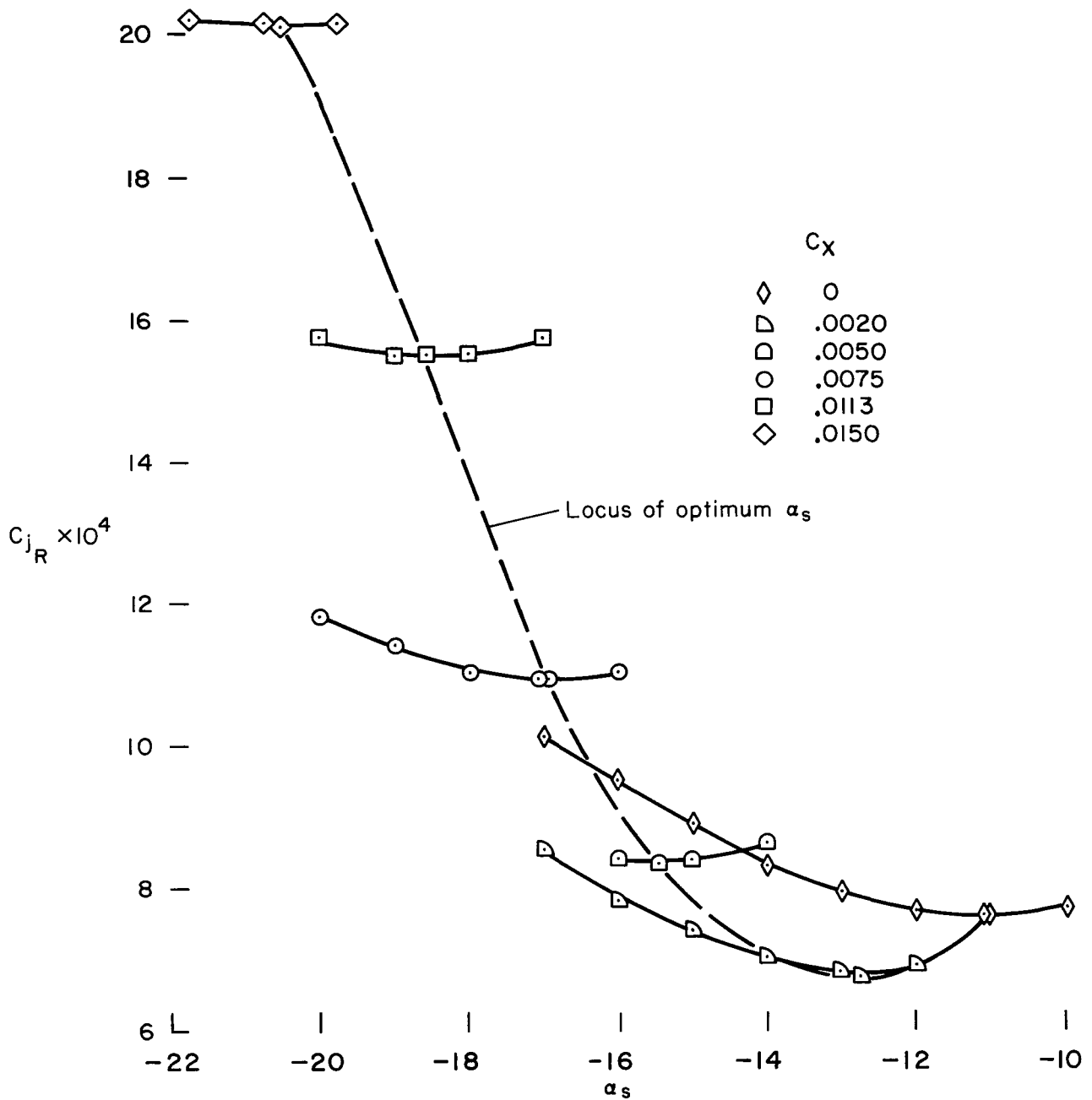
(b) Effects on control requirements and blade flapping (see also fig. 4(b)).

Figure 8.- Continued.



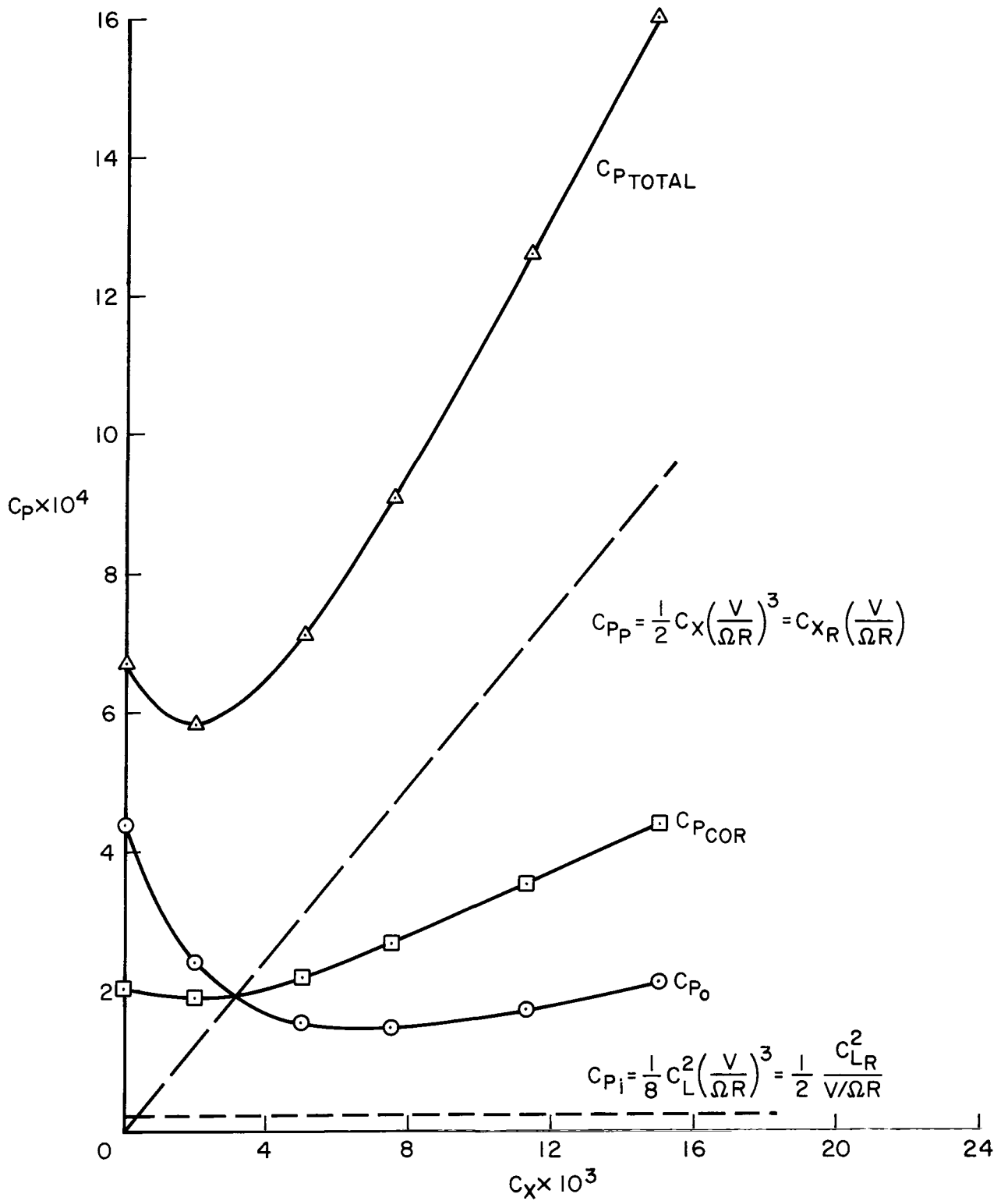
(c) Effects on power components at optimum shaft angles.

Figure 8.- Concluded.



(a) Effects on the variation of C_{j_R} vs α_s .

Figure 9.- Effects of propulsive force for the jet-flap rotor; $C_{L_R} = 0.00488$, $V/\Omega R = 0.5$, $\theta_{0.7} = 12^\circ$, $\Omega R = 591$ ft/sec.



(b) Power components for optimum data of figure 9(a).

Figure 9.- Concluded.

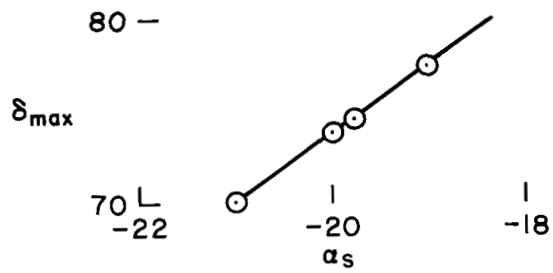


Figure 10.- Jet deflections for the data at highest C_X shown in figure 9 ($C_X = 0.015$); $C_{LR} = 0.00488$, $V/\Omega R = 0.5$, $\theta_{0.7} = 12^\circ$, $\Omega R = 591$ ft/sec.

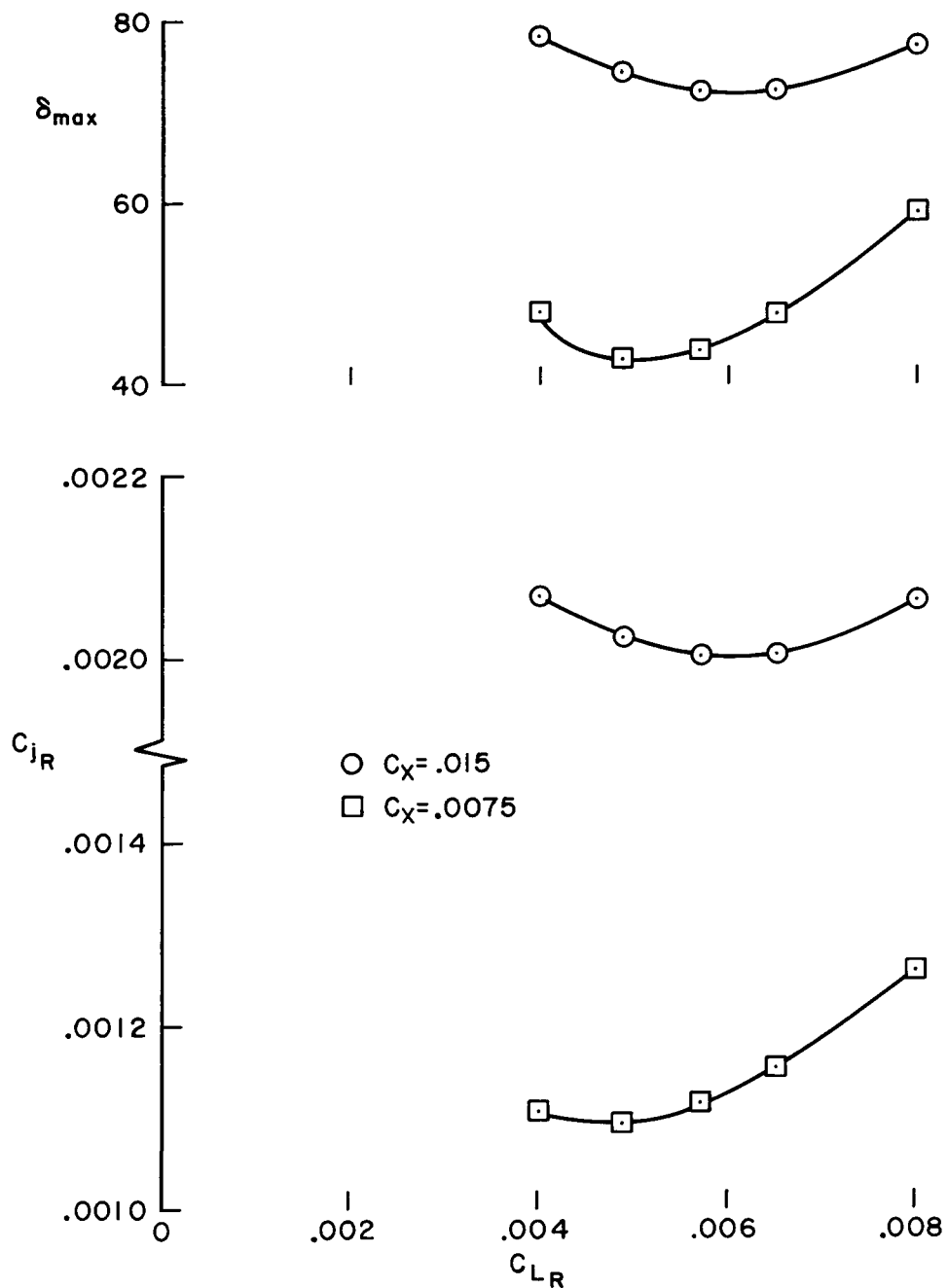


Figure 11.- Effects of C_{LR} for the jet-flap rotor at optimum shaft angles for two values of C_X ; $V/\Omega R = 0.5$, $\theta_{0.7} = 12^\circ$, $\Omega R = 591$ ft/sec.

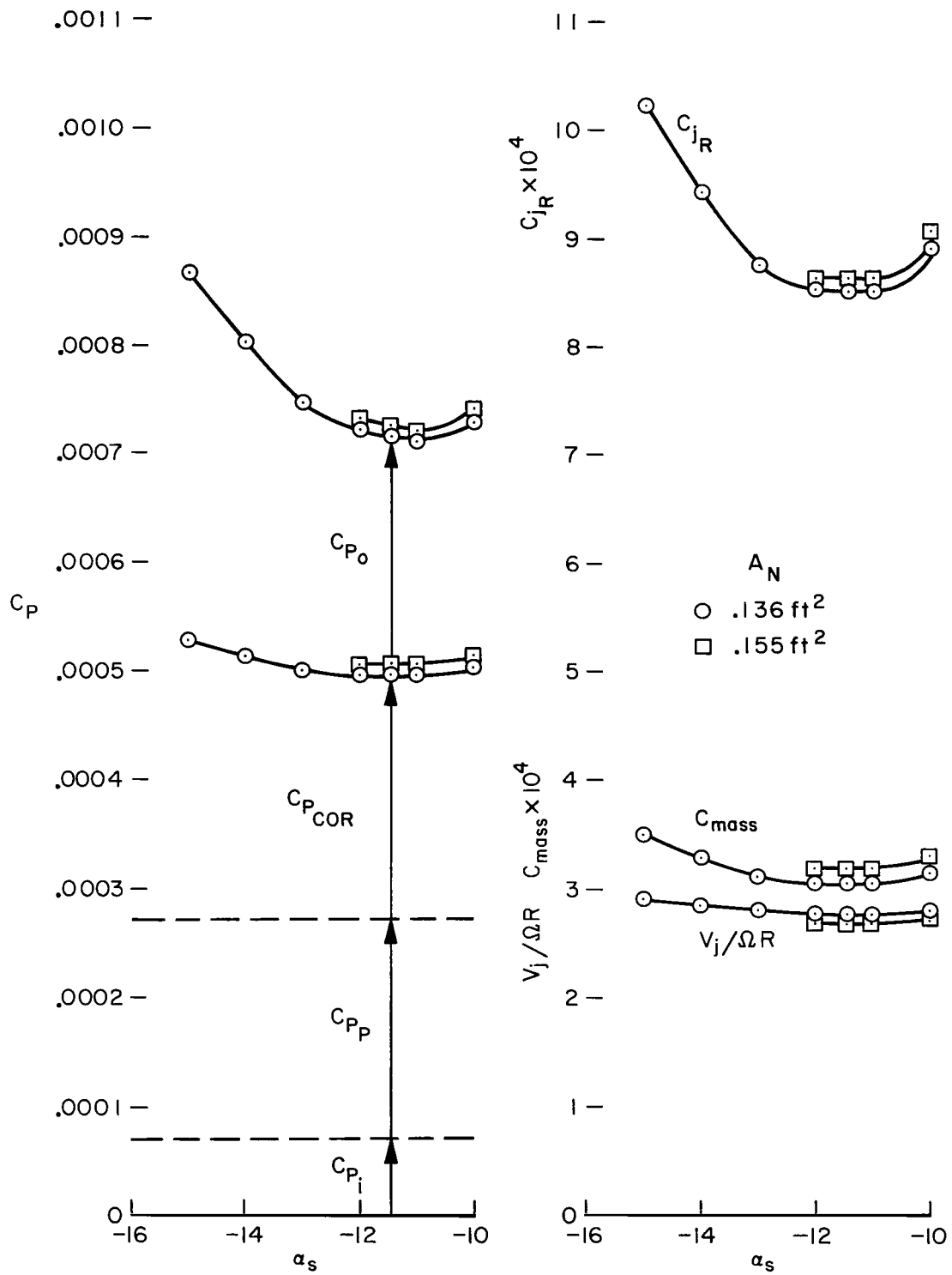
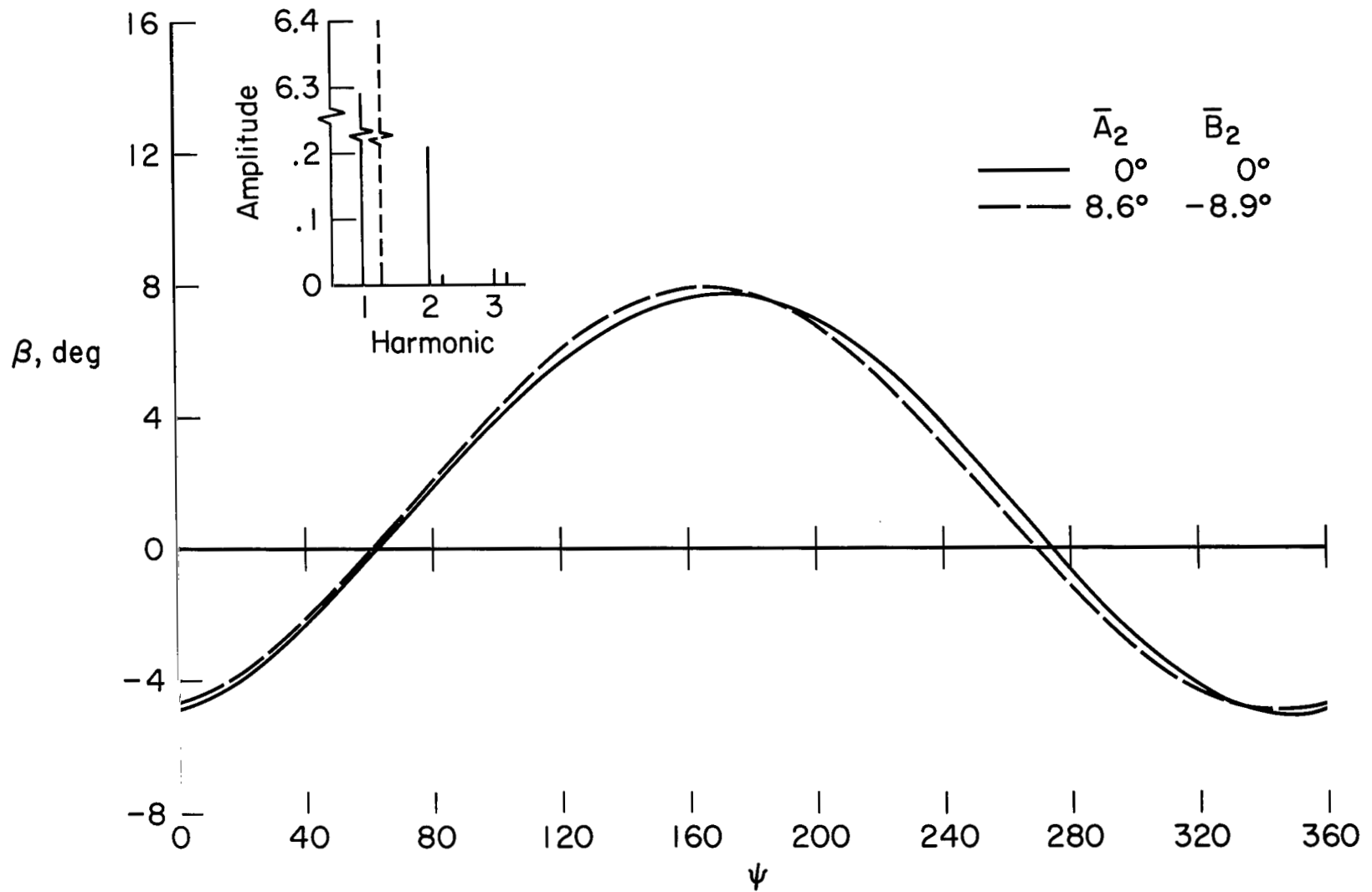
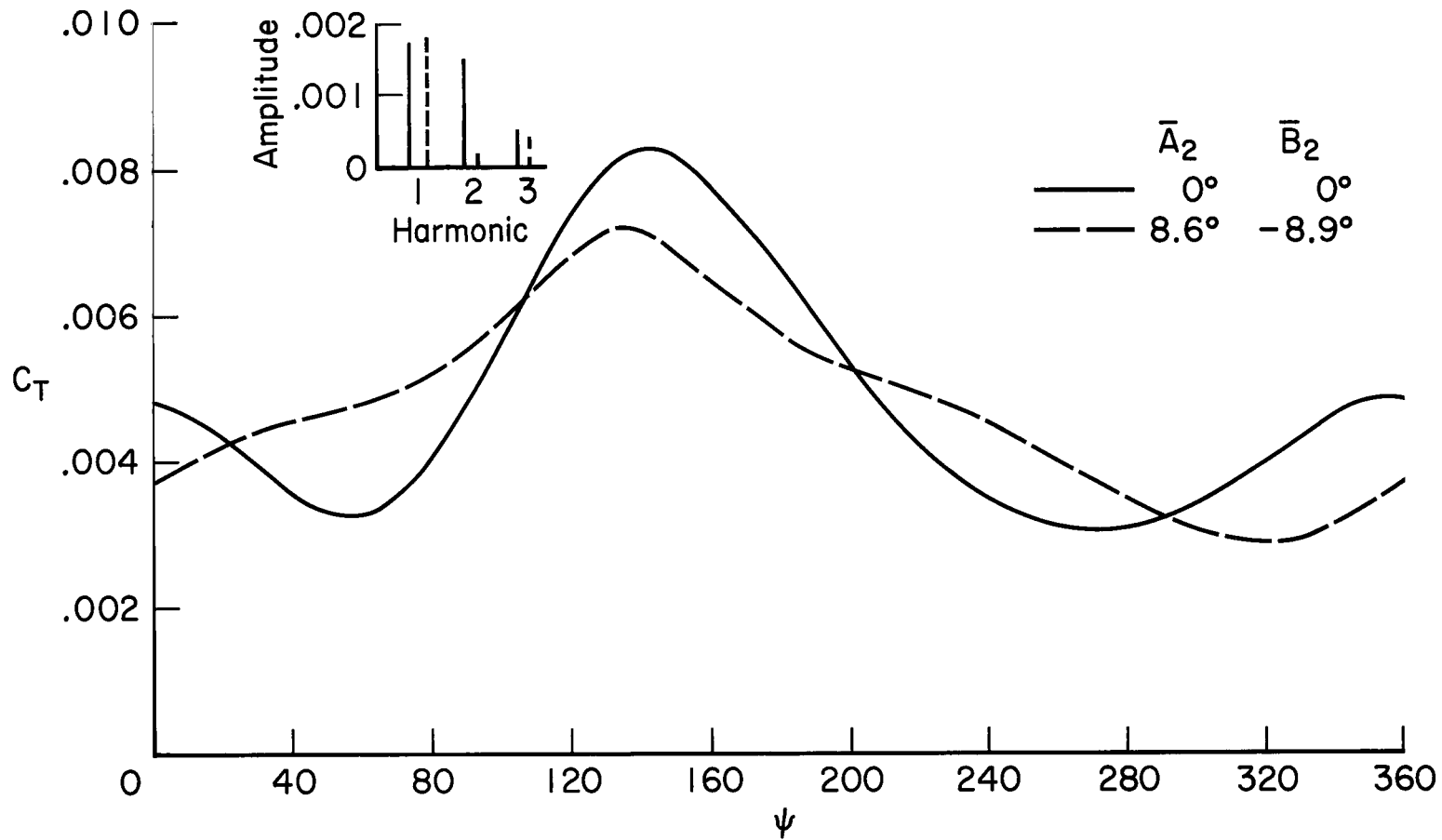


Figure 12.- Effects of nozzle area for the jet-flap rotor; $C_{LR} = 0.0065$, $C_X = 0.015$, $V/\Omega R = 0.3$, $\theta_{0.7} = 12^\circ$, $\Omega R = 591 \text{ ft/sec}$.



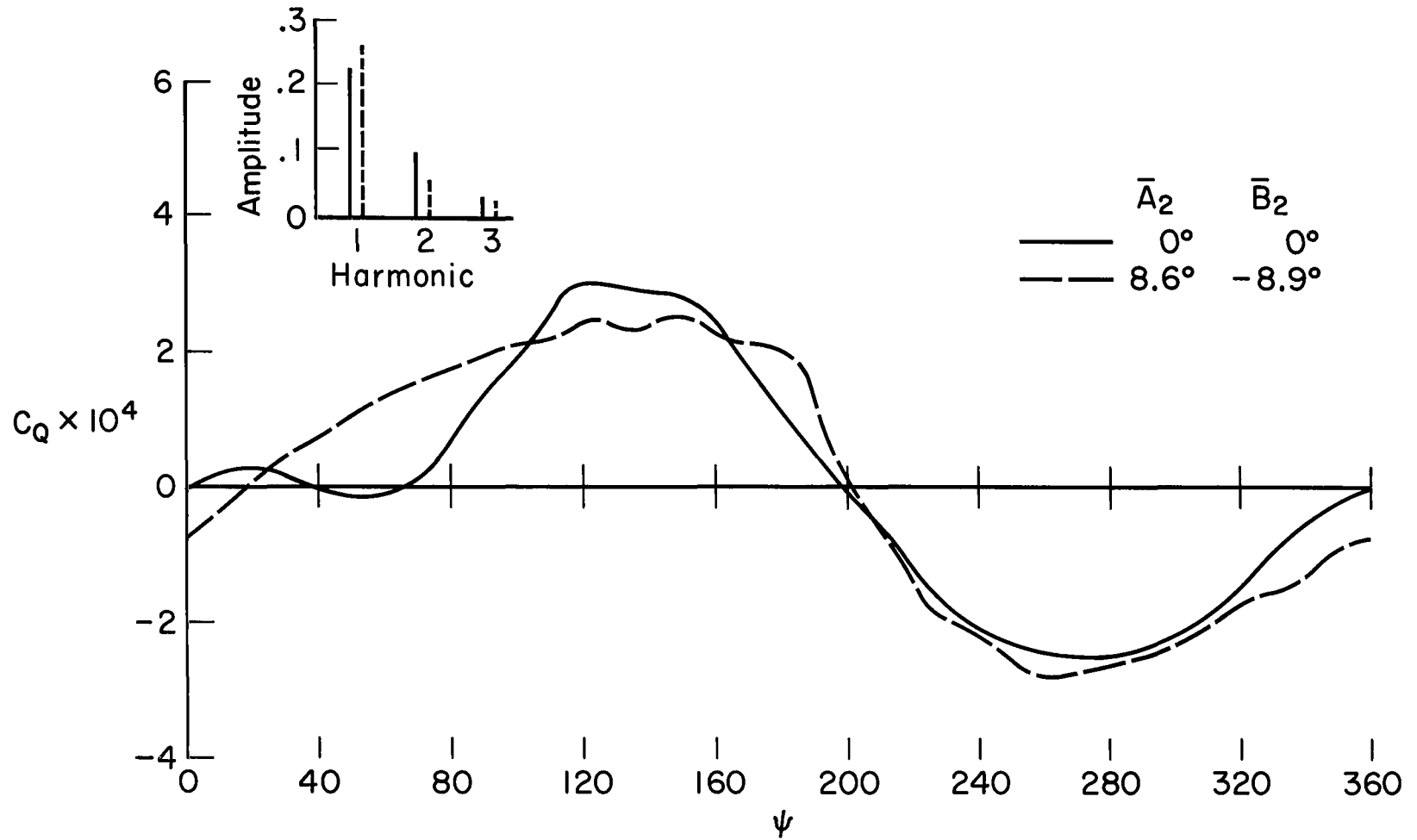
(a) Effects on blade flapping.

Figure 13.- Effects of second harmonic control.



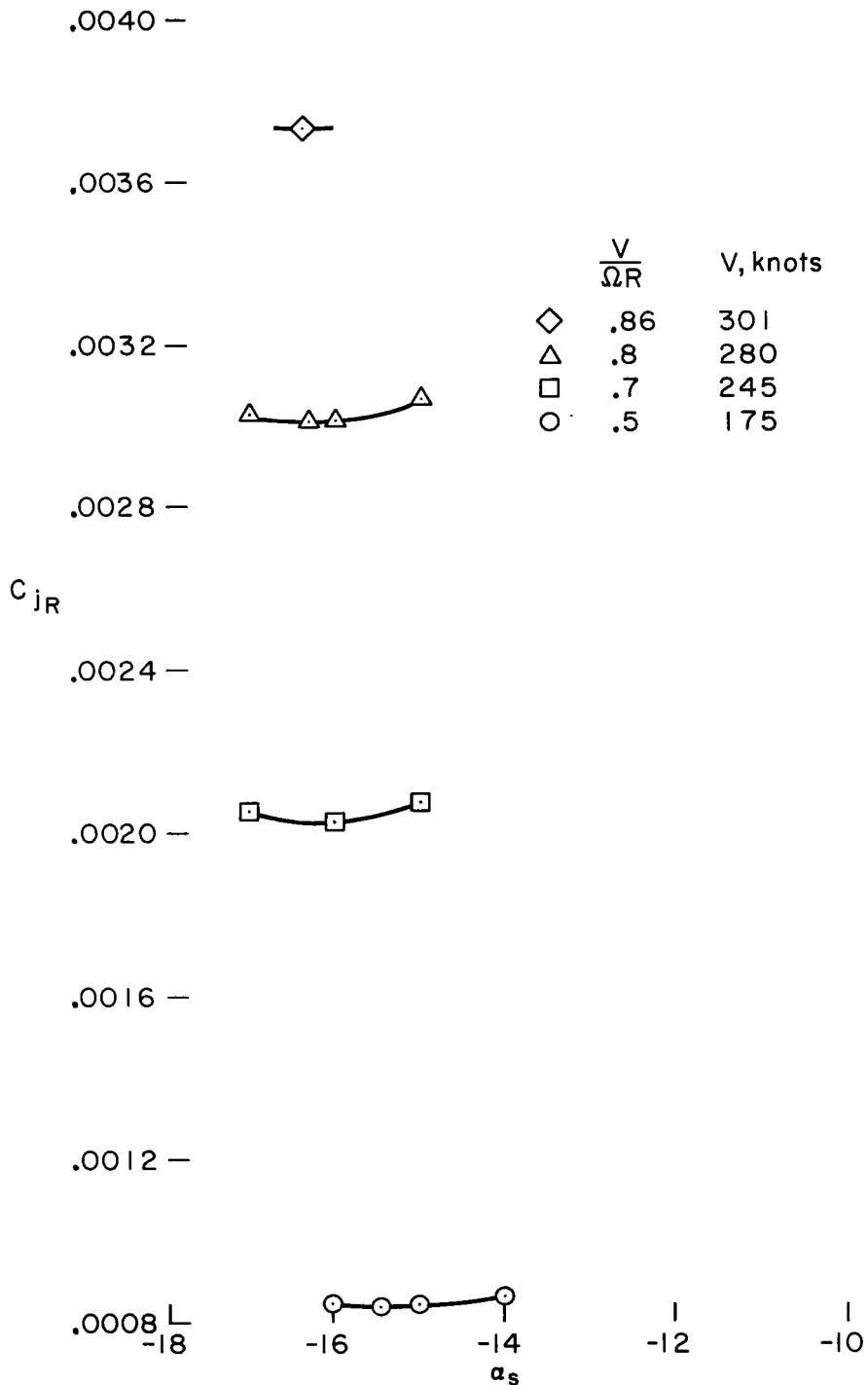
(b) Effects on thrust distribution.

Figure 13.- Continued.



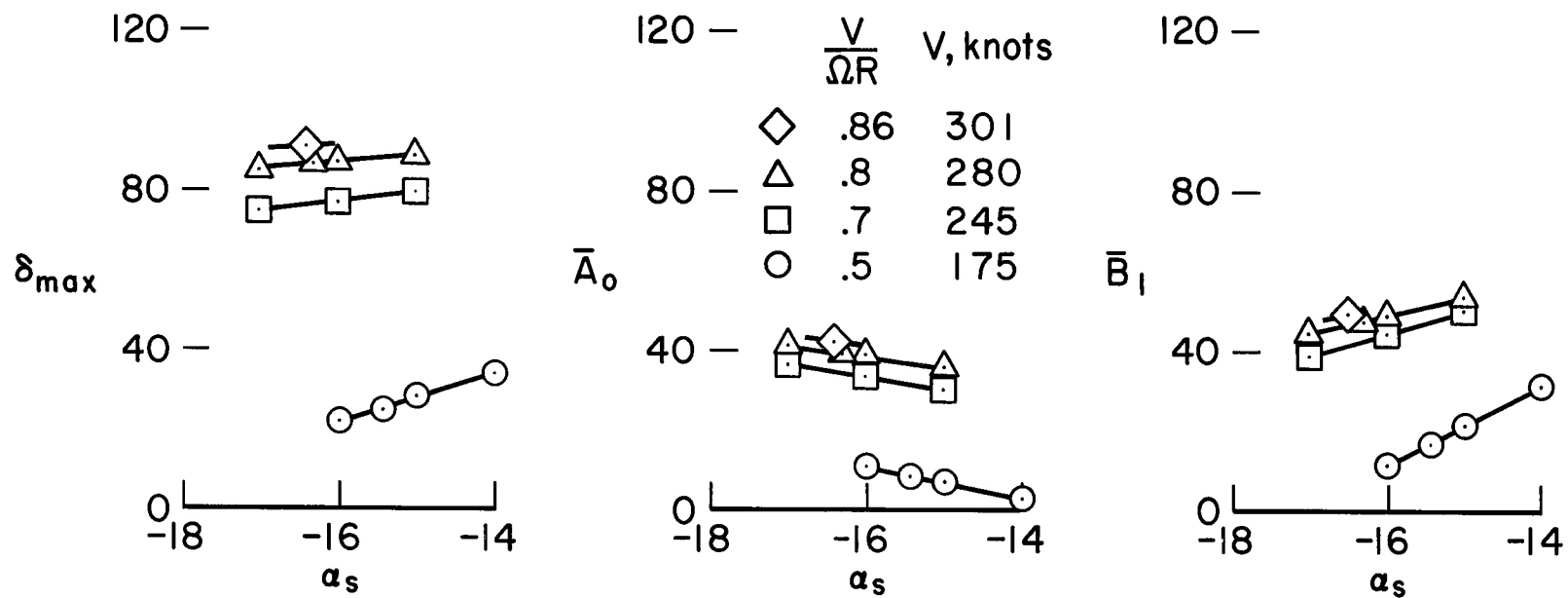
(c) Effects on torque distribution.

Figure 13.- Concluded.



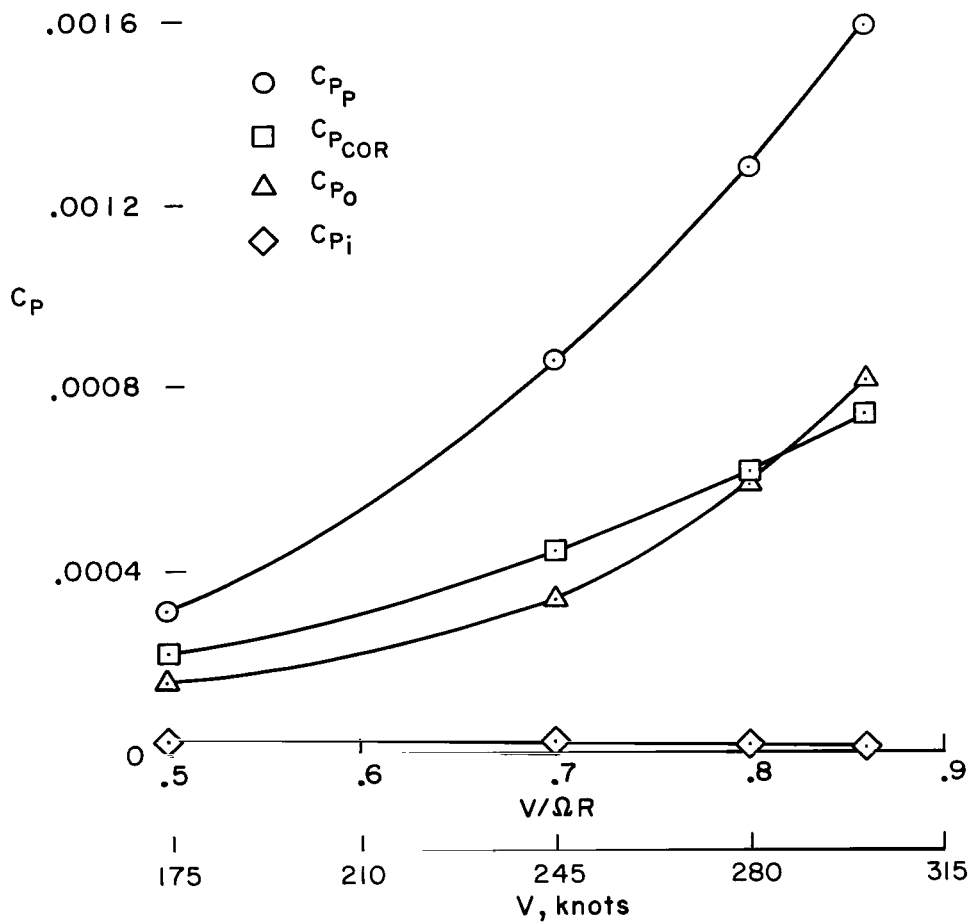
(a) Effects on momentum coefficient.

Figure 14.- Effects of high advance ratio; $C_{LR} = 0.00488$, $C_X = 0.005$, $\theta_{0.7} = 12^\circ$, $\Omega R = 591$ ft/sec.



(b) Effects on jet-deflection control requirements.

Figure 14.- Continued.



(c) Effects on power components at optimum shaft angles.

Figure 14.- Concluded.

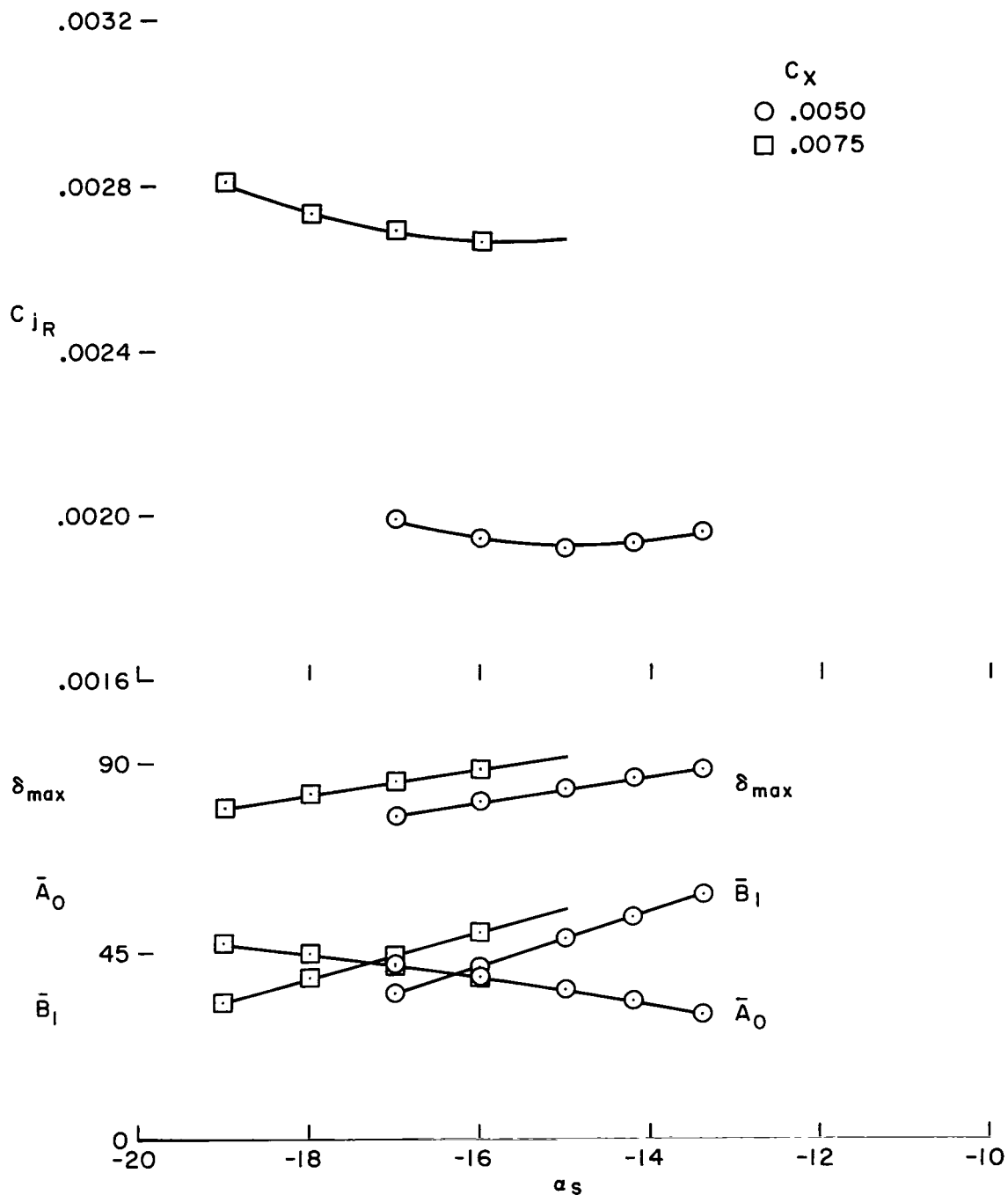


Figure 15.- Selected characteristics of the jet-flap rotor at a forward speed of 220 knots and an advancing tip Mach number of 0.8; $V/\Omega R = 0.7$, $\Omega R = 531$ ft/sec, $\theta_{0.7} = 12^\circ$, $C_{LR} = 0.006025$.

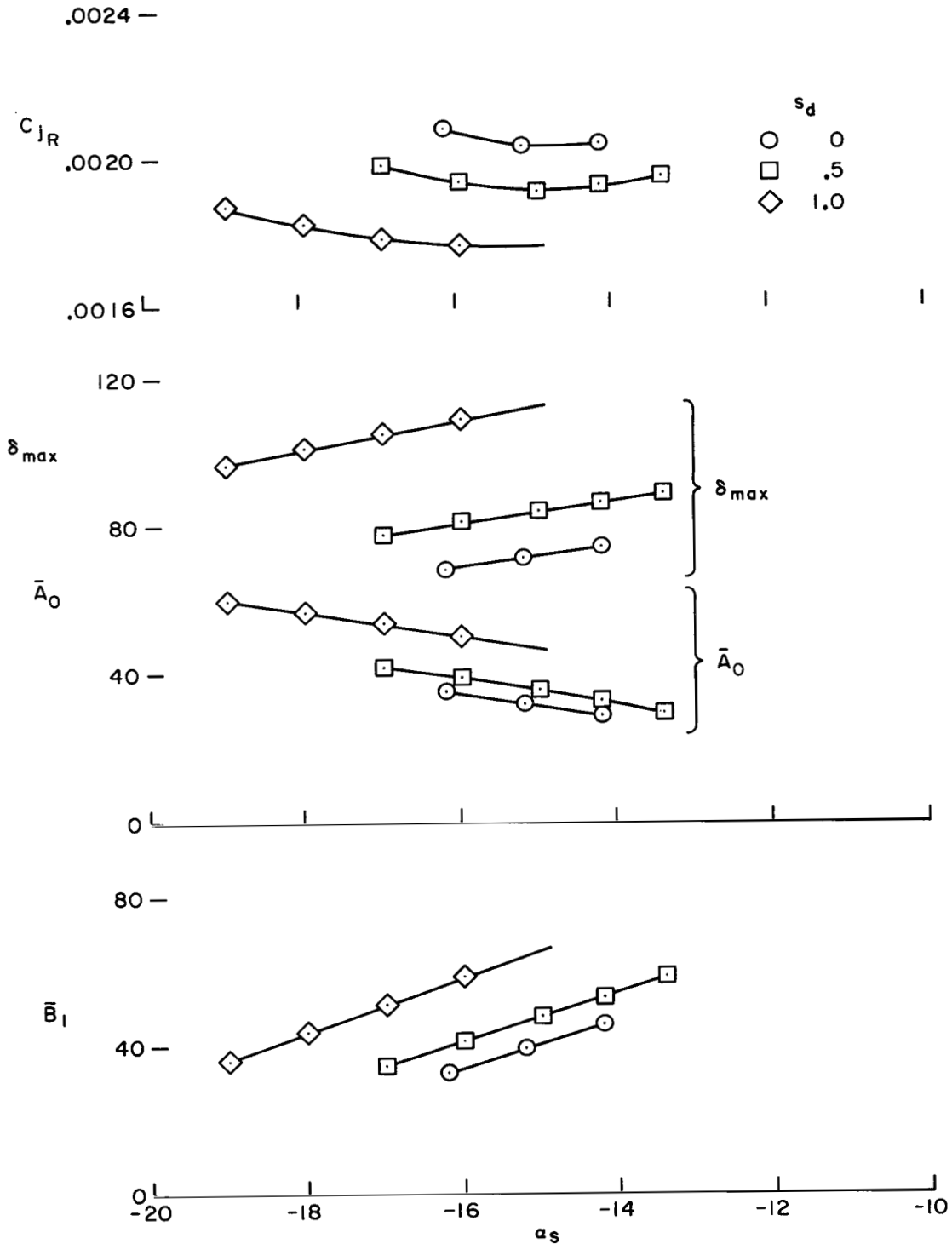
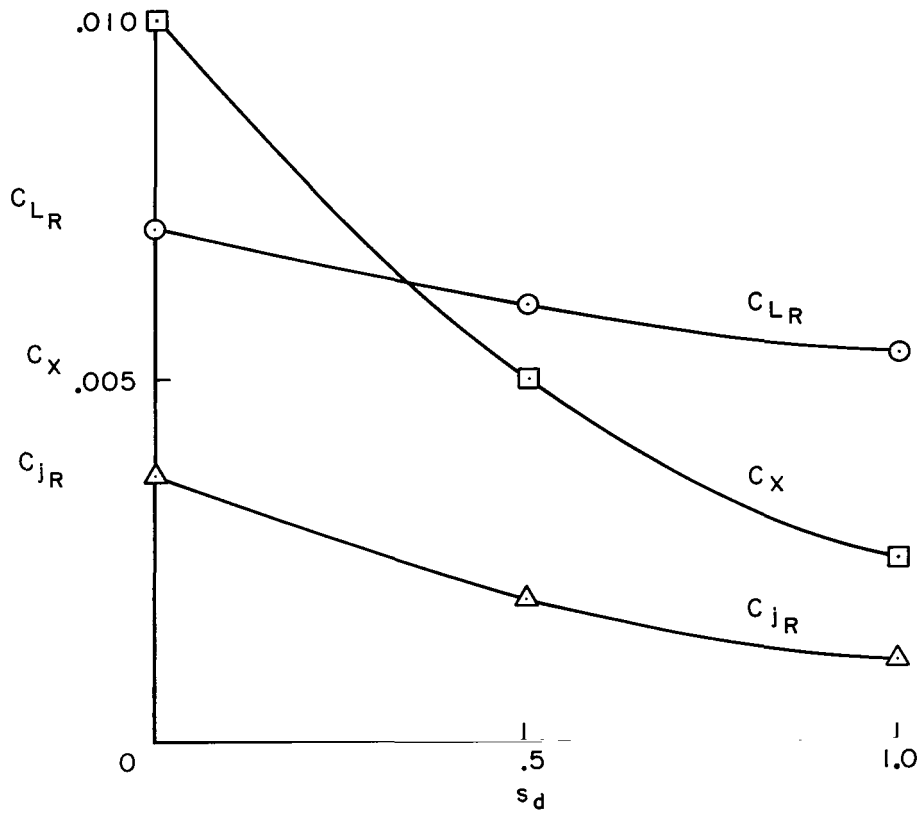
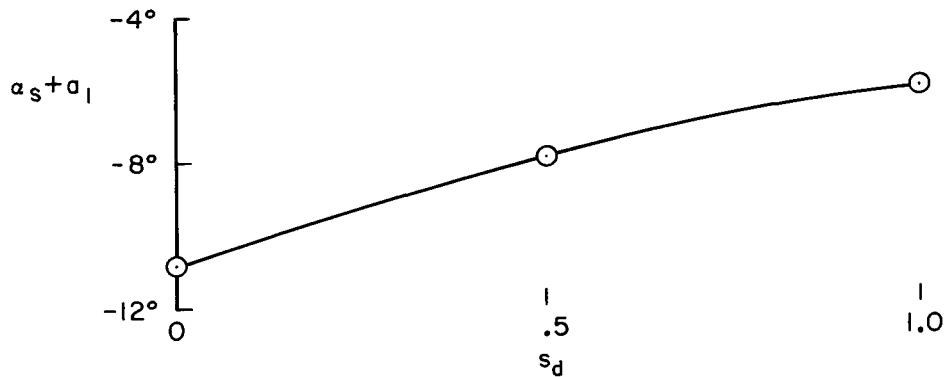


Figure 16.- Effects of the thrust recovery parameter s_d for the least-propulsive-force condition of figure 15; $C_{LR} = 0.006025$, $C_X = 0.005$, $\theta_{0.7} = 12^\circ$, $\Omega R = 531$ ft/sec, $V/\Omega R = 0.7$.



(a) Effects on force coefficients.



(b) Effect on tilt of the rotor disk.

Figure 17.- Effects of s_d at fixed shaft angle and control settings;
 $\alpha_s = -14.2$, $\bar{A}_0 = 33.0$, $\bar{B}_1 = 53.4$, $V/\Omega R = 0.7$, $\theta_{0.7} = 12^\circ$, $\Omega R = 531$ ft/sec.

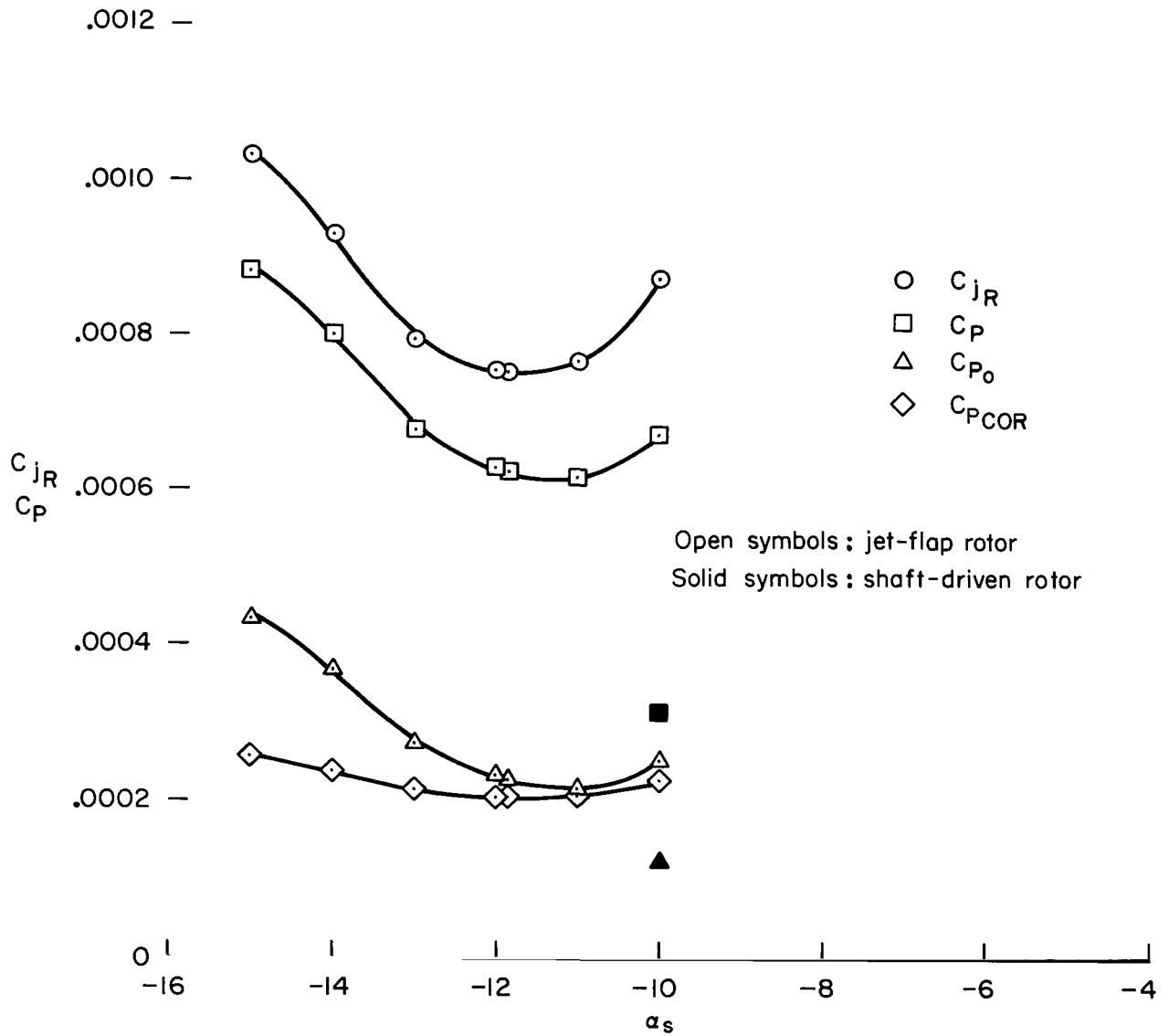


Figure 18.- Comparison of the jet-flap and shaft-driven rotors for the same flight condition; $C_{LR} = 0.00488$, $C_X = 0.0113$, $V/\Omega R = 0.3$, $\Omega R = 591$ ft/sec.

3/17/25
67

"The aeronautical and space activities of the United States shall be conducted so as to contribute . . . to the expansion of human knowledge of phenomena in the atmosphere and space. The Administration shall provide for the widest practicable and appropriate dissemination of information concerning its activities and the results thereof."

—NATIONAL AERONAUTICS AND SPACE ACT OF 1958

NASA SCIENTIFIC AND TECHNICAL PUBLICATIONS

TECHNICAL REPORTS: Scientific and technical information considered important, complete, and a lasting contribution to existing knowledge.

TECHNICAL NOTES: Information less broad in scope but nevertheless of importance as a contribution to existing knowledge.

TECHNICAL MEMORANDUMS: Information receiving limited distribution because of preliminary data, security classification, or other reasons.

CONTRACTOR REPORTS: Technical information generated in connection with a NASA contract or grant and released under NASA auspices.

TECHNICAL TRANSLATIONS: Information published in a foreign language considered to merit NASA distribution in English.

TECHNICAL REPRINTS: Information derived from NASA activities and initially published in the form of journal articles.

SPECIAL PUBLICATIONS: Information derived from or of value to NASA activities but not necessarily reporting the results of individual NASA-programmed scientific efforts. Publications include conference proceedings, monographs, data compilations, handbooks, sourcebooks, and special bibliographies.

Details on the availability of these publications may be obtained from:

SCIENTIFIC AND TECHNICAL INFORMATION DIVISION
NATIONAL AERONAUTICS AND SPACE ADMINISTRATION
Washington, D.C. 20546